Cable-driven parallel robot for curtain wall module installation

K. Iturralde [a,*], M. Feucht [a], D. Illner [a], R. Hu [a], W. Pan [a], T. Linner [a], T. Bock [a], I. Eskudero [b], M. Rodriguez [b], J. Gorrotxategi [b], J.B. Izard [b], J. Astudillo [b], J. Cavalcanti Santos [c], M. Gouttefarde [c], M. Fabritius [d], C. Martin [d], T. Henninge [e], S.M. Normes [e], Y. Jacobsen [e], A. Pracucci [f], J. Cañada [g], J.D. Jimenez-Vicaria [h], R. Alonso [i], L. Elia [i]

[a] *Chair of Building Realization and Robotics, Technical University of Munich, Germany*
[b] *TECNALIA, Basque Research and Technology Alliance (BRTA), Spain*
[c] *LIRMM, Univ Montpellier, CNRS, France*
[d] *IPA, Fraunhofer, Germany*
[e] *nLink, Norway*
[f] *Focchi Spa, Italy*
[g] *Vicinay-Cemvisa, Spain*
[h] *Acciona, Spain*
[i] *R2M Solution, United Kingdom*

ARTICLE INFO

ABSTRACT

A cable-driven parallel robot (CDPR) was developed for the installation of curtain wall modules (CWM). The research addressed the question of whether the CDPR was capable installing CWMs with sufficient accuracy while being competitive compared to conventional manual methods. In order to develop and test such a system, a conceptual framework that consisted of three sub-systems was defined. The tests, carried out in two close-to-real demonstration buildings, revealed an absolute accuracy of the CWM installation of 4 to 23 mm. The working time for installing a CWM was reduced to 0.51 h. The results also show that the system is competitive for a workspace greater than 96 m^2 compared to conventional manual methods. However, improvements such as reducing the hours for setting up the CDPR on the one hand and achieving a faster and more robust MEE on the other hand will be still necessary in the future.

1. Introduction

Curtain wall modules (CWMs) are prefabricated building envelope systems that represent the boundary conditions between the indoor and outdoor environments with the goal of guaranteeing and preserving the designed building performance. For this purpose, the as-built façade must guarantee the correct installation of the CWMs in order to achieve the performance defined by project specifications, detailed in the design phase and validated with tests conducted under standards such as EN 13830:2005 [1](environmental and mechanical tests), ISO 16283-3:2016 [2] and ISO 717-1:2013 [3] (airborne sound insulation), ISO 10848:2017 [4] (flanking transmission) as well as other laboratory tests. The growing trend of off-site prefabrication of CWMs (which reduces on-site activities, time for installation, and overall costs as well as higher quality of the building envelope) makes the installation process the key

phase to fully accomplish project specifications and operative instructions. Moreover, it guarantees the performance achievement with a strict accuracy. Because the installation of CWMs requires a high degree of accuracy to ensure proper building performance, the installation process and regulations guarantee that the as-built façade corresponds to the design. For this reason, although regulations of some specific façade components (e.g., bolts, screws, anchors, etc.) are possible, installers today still perform a crucial role. In addition to the installation operations to ensure the correct setting of CWMs in line with project specifications, other relevant issues concerning site activities need to be managed, such as risk control to ensure the safety of personnel involved and correct maintenance of the equipment used. The safety of personnel involved in all site activities (not only those who are responsible for the façade) is the most crucial aspect. Safety procedures are independent of specific building components but related to the general principles

---

* Corresponding author.
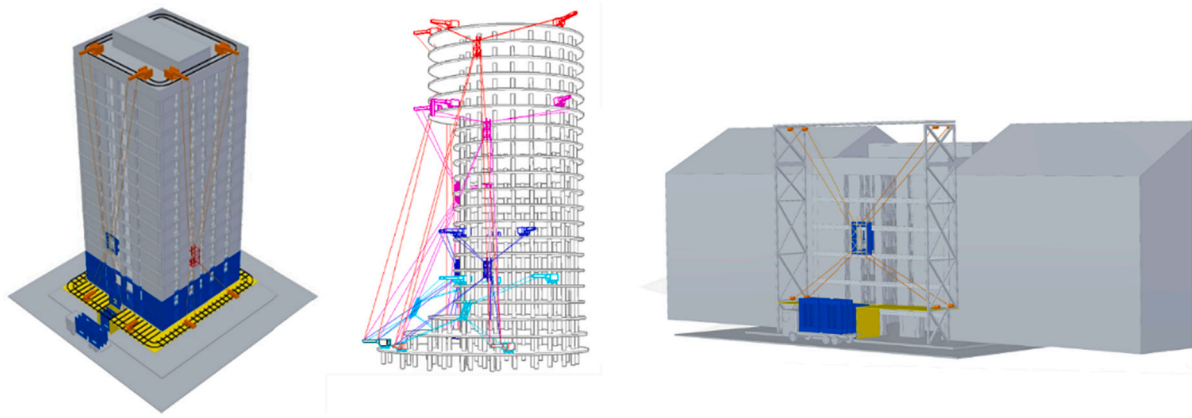 *E-mail address:* kepa.iturralde@br2.ar.tum.de (K. Iturralde).

Fig. 1. Façade renovation with modules for a high-rise building (left), CDPR for high rise erection (middle), façade renovation with modules for a low-rise building (right) [37].
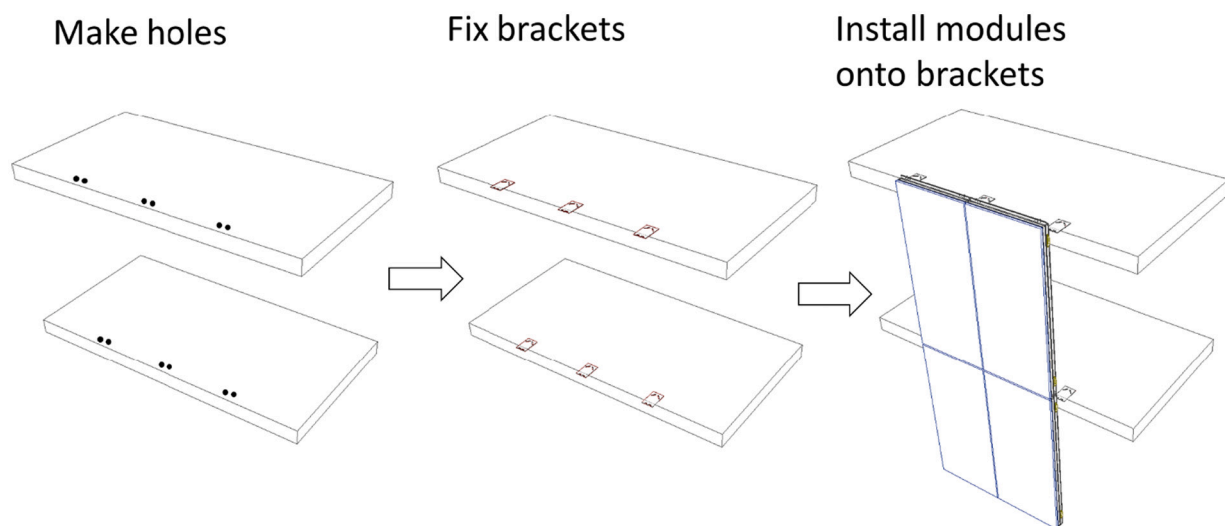

Fig. 2. Installation process of the curtain wall, schematic process.
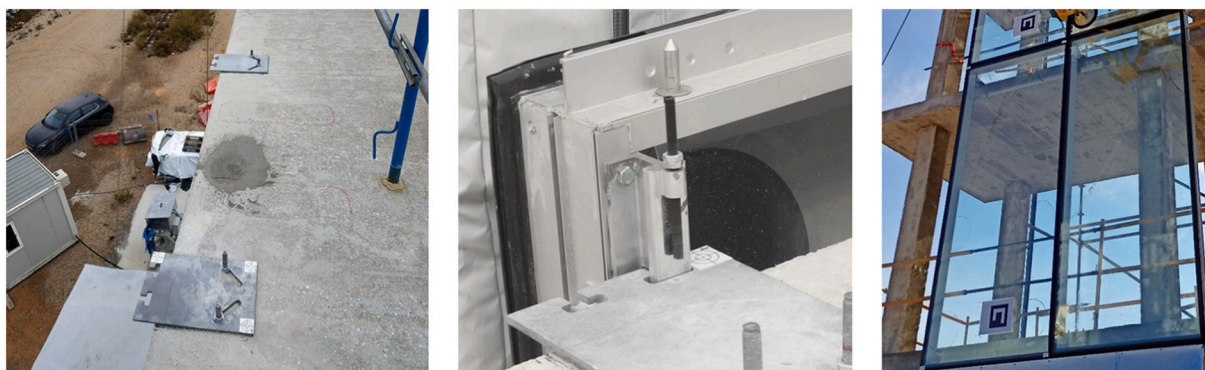

Fig. 3. Brackets installed (left), CWM being installed onto bracket (middle) [36], CWM modules installed on top of the brackets (right).

applied to each site activity based on national and local norms. Specifically, façade related risks (e.g., lifting materials, equipment placement, exclusion zones, falling restraints for personnel and material, weather conditions during lifting operations) are some of the risks to be considered during the CWM installation. Therefore, to maintain the quality of installation while reducing the safety risks for site personnel, automation and robotics present an opportunity worth investigating.

In the past, different robots were developed for installing, painting, cleaning, delaminating, maintaining and inspecting any kind of facade. More specifically, several robotic devices were categorized for façade module installation [5]. Besides these single task robots, techniques for installing fully prefabricated façade modules during the erection of new buildings were developed in on-site construction factories such as ABCS [6] and SMART [7,8]. Apart from façade modules, there were
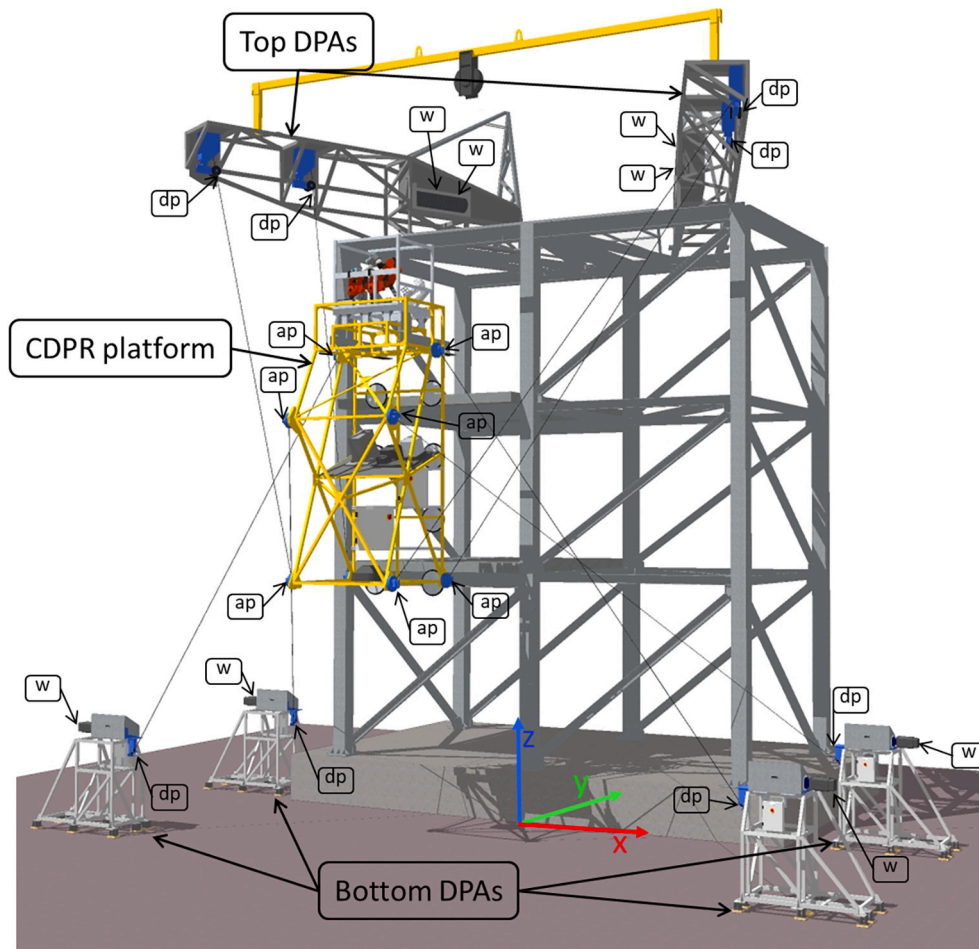
Fig. 4. CAD view of the Hephaestus CDPR prototype on the first demonstration building at Tecnalia's facilities.

Table 1
WFTW limit coordinates. Applies throughout X = [−3.5; 3.5].

	TRANSIT OF CWM						PICKING POSITION OF CWM					
Y	−0.75	−0.98	−1.15	−1.21	−1.44	−1.67	−1.75	−1.90	−2.13	−2.36	−2.59	−2.83
Z	7.79	9.31	10.20	10.56	11.86	10.97	10.35	9.15	7.55	6.20	4.90	3.68

experiences in on-site assembly of walls such as the ROCCO project (specifically for assembling building blocks) [9]. Lee et al. [10] developed a robot on a platform to assist the human operator handle a CWM. The most recent instance of façade module installation with a robot was a manually operated robotic crane [11]. Test results showed that the achieved repeatable accuracy of the handler end-effector positioning is 7.0 mm in a worst case scenario. This result might not be sufficient for the installation of CWMs. Regarding the CDPRs for installing façade elements, a tendon-suspended platform robot was envisioned [12], but its definition lacked further detail, especially regarding the necessary cranes to support cable loads and forces. Moreover, this solution did not show any type of on-board tools.

Cable-driven parallel robots (CDPR) represent a subclass of parallel robots [13–15]. Instead of rigid links, cables are used to manipulate a mobile platform. The principle involves driving the mobile platform in up to six degrees of freedom (DOF) by attaching cables to the mobile platform and by synchronously controlling their length from a base frame with winches. At least six cables are required for controlling all 6DOFs of the load [16,17], while often no more than 8 cables are used for better performance [18,19]. The most well-known example of such robots is the aerial camera for stadiums [20] with 3 DOFs and 4 cables,

and the first concept for manipulating all DOFs of a load dates back to the late 1980s and beginning of 1990s [16,21]. Today, their benefits have already been proven, in particular for large scale industrial applications [18,19,22–25]. Naturally, the principle of a CDPR can be adapted to move heavy payloads on a large scale. For the same reasons, CDPRs have being envisioned in the past for several construction applications from manipulating elements, contour crafting, to building inspection [12,26]. However, only a few related instances involving CDPRs in the field of construction can be found. In [27], a concept of a CDPR for large-scale assembly of solar power plants was introduced. Bosscher et al. proposed a CDPR for a contour crafting system [28]. Schröeder proposed a cable robot prototype to maintain vertical green facades [29]. In [30–32], CDPRs for automated brick laying were reported. Merlet developed Marionet, the modular wire-driven parallel robots [33] that were used in collaboration with the artist Anne-Valérie Gasc for the 3D printing of large landscape type volumes [34].

The Hephaestus project proposed [35,36] the use of a CDPR for the installation of CWMs. The 6DOF of the mobile platform were redundantly constrained using eight cables, which is a well-known choice when a large workspace is necessary [19,20]. In the preliminary stages of the research project, the concept was designed to use the CDPR for
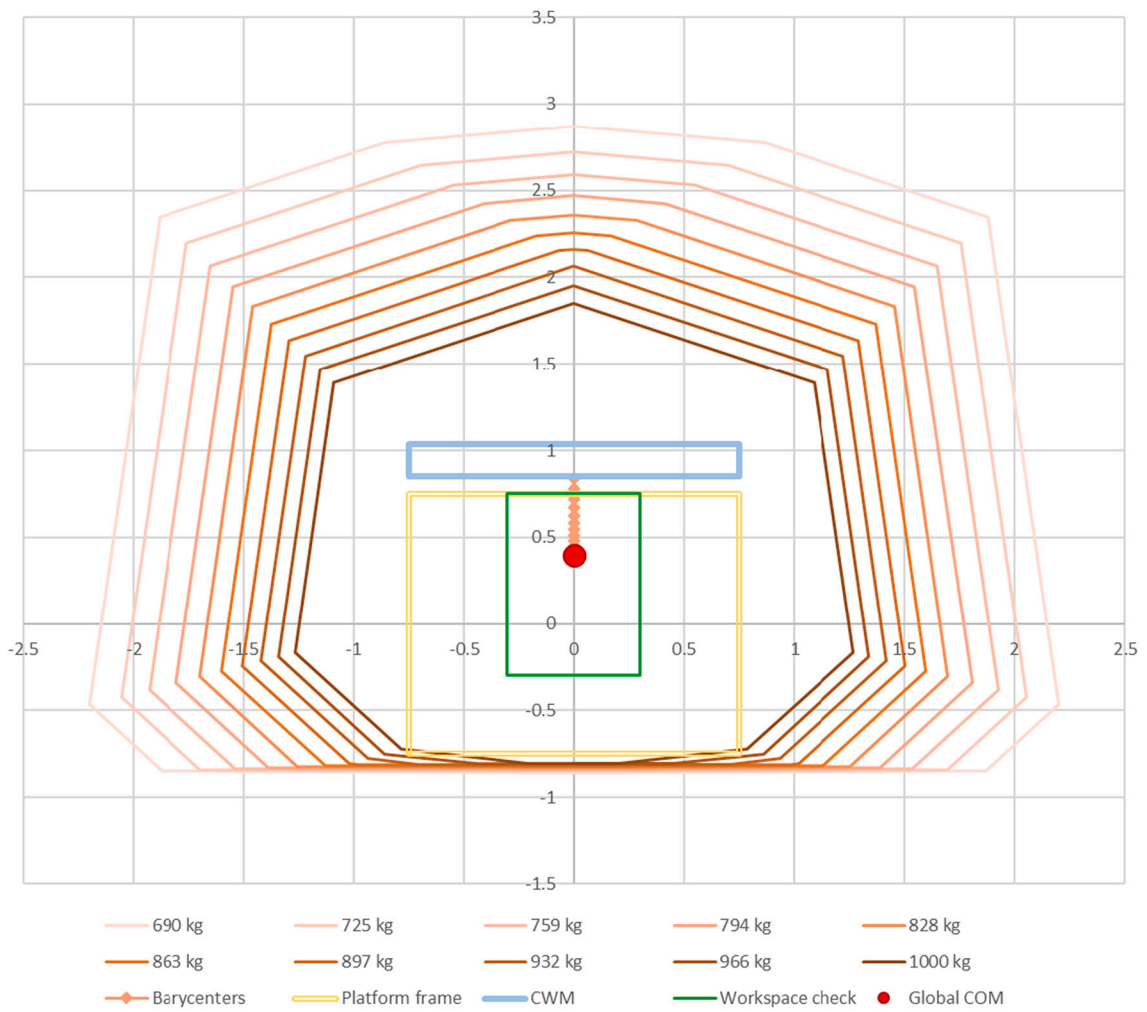
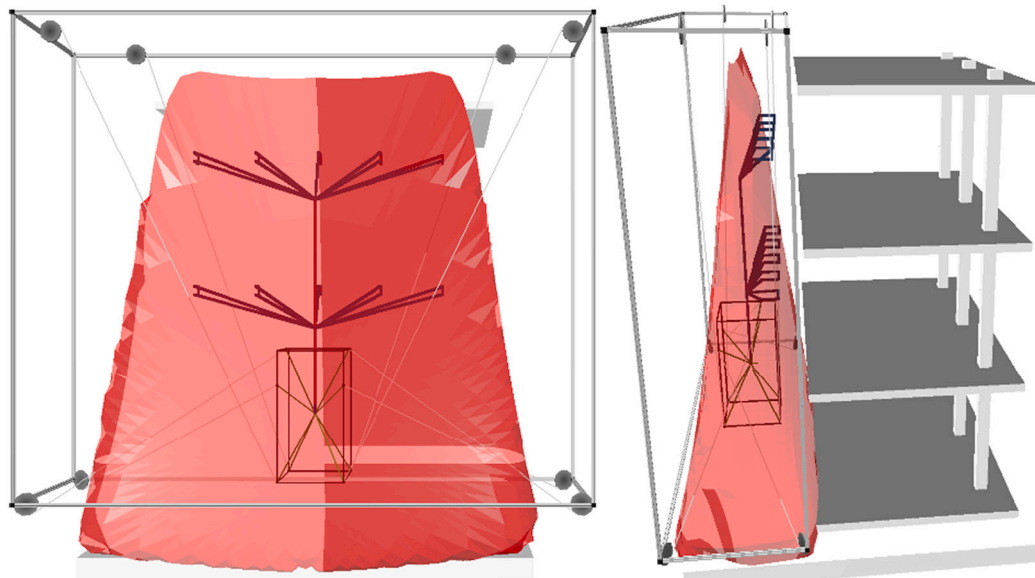**Fig. 5.** Polygons of stability on a top view of the platform.

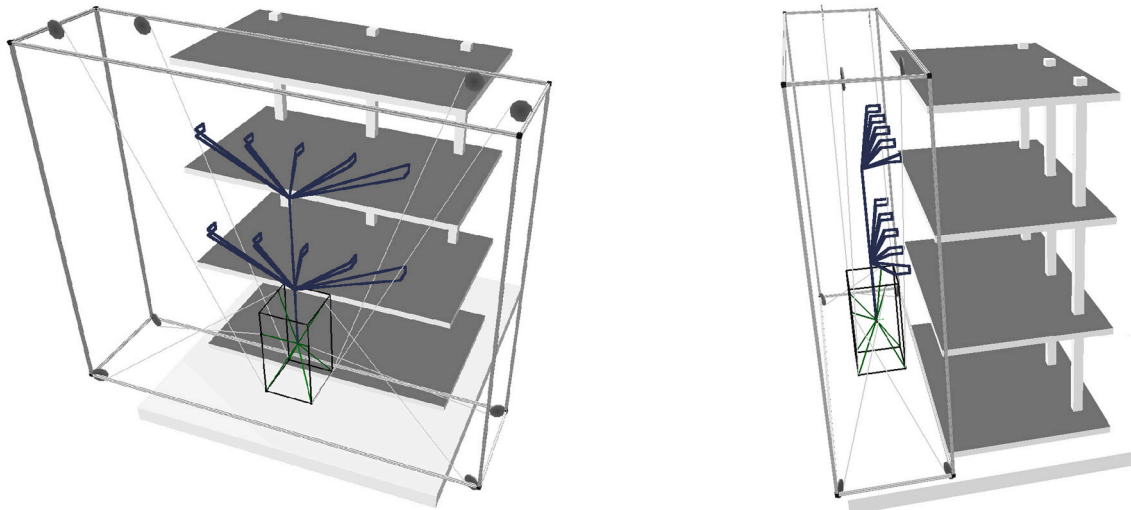**Fig. 7.** Workspace calculated through the simulation.

Fig. 6. Simulation of the robot movement based on a trajectory to mount several CWMs.
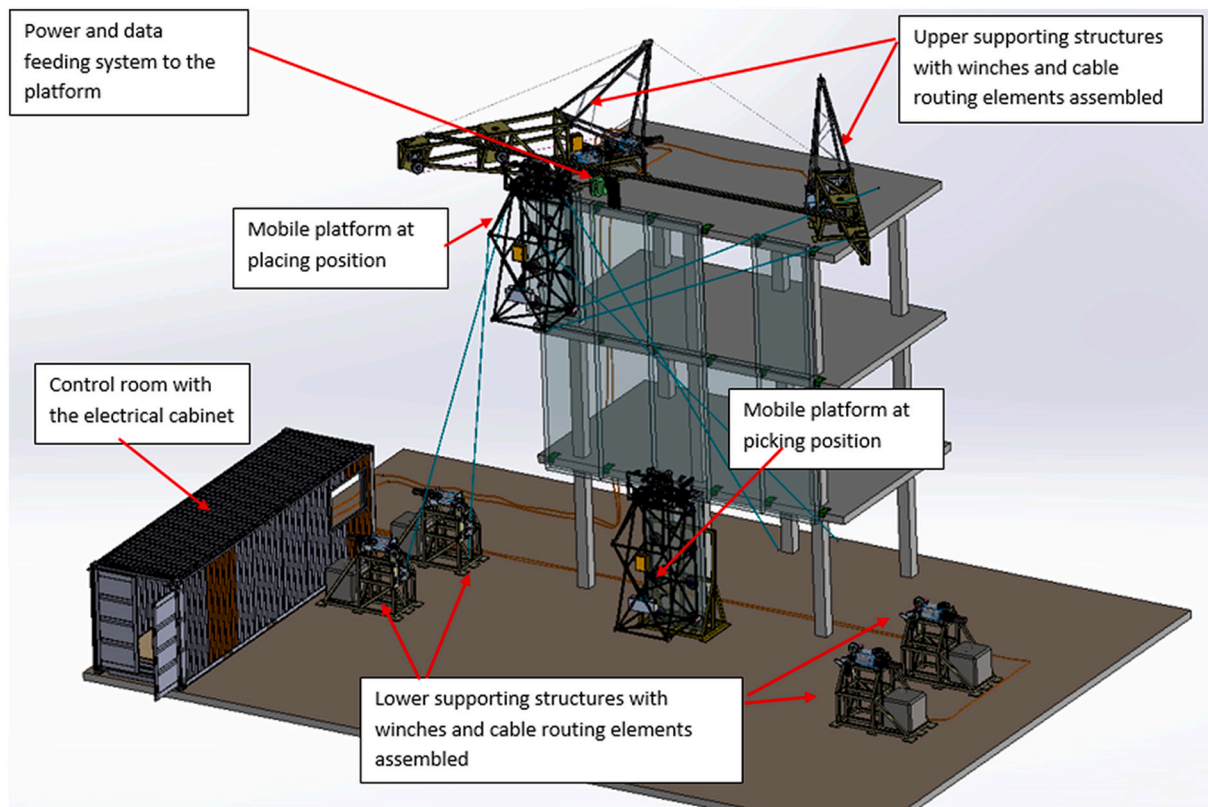

Fig. 8. 3D CAD view of the whole Hephaestus system for the second demonstration building at Acciona's facilities.

different tasks related to the vertical envelope of a building [37]. The initial concepts included renovation activities on façades. In scenarios where the existing building conditions would not allow for renovation activities, such activity would require a supporting structure independent of the existing building to hold the CDPR (Fig. 1 right).

The initial ideas evolved and the Hephaestus research project [35] finally focused on the installation of CWMs. There are specific requirements for the installation of a CWM. A CWM is a prefabricated façade module that consists of a frame (typically in aluminum) and a glass panel in the middle. In the case of HEPHEASTUS, the CWM weighed about 300 kg. The CWM hangs from two brackets on the

concrete building slab and the gaskets between the joints of the units ensure water resistance and airtightness when the modules are placed beside each other, as illustrated in Figs. 2 and 3. The brackets are fixed to the concrete slab with screws. The CWM manual installation process requires marking the location of the brackets by using Total Station theodolites.

The work performed through the Hephaestus project [36] featured for the first time a CDPR that was designed, built and deployed specifically for the construction sector, with the primary purpose of installing CWMs and comprising two main tasks: brackets installation and CWM placement. The advantages of CDPRs in Hephaestus were their large
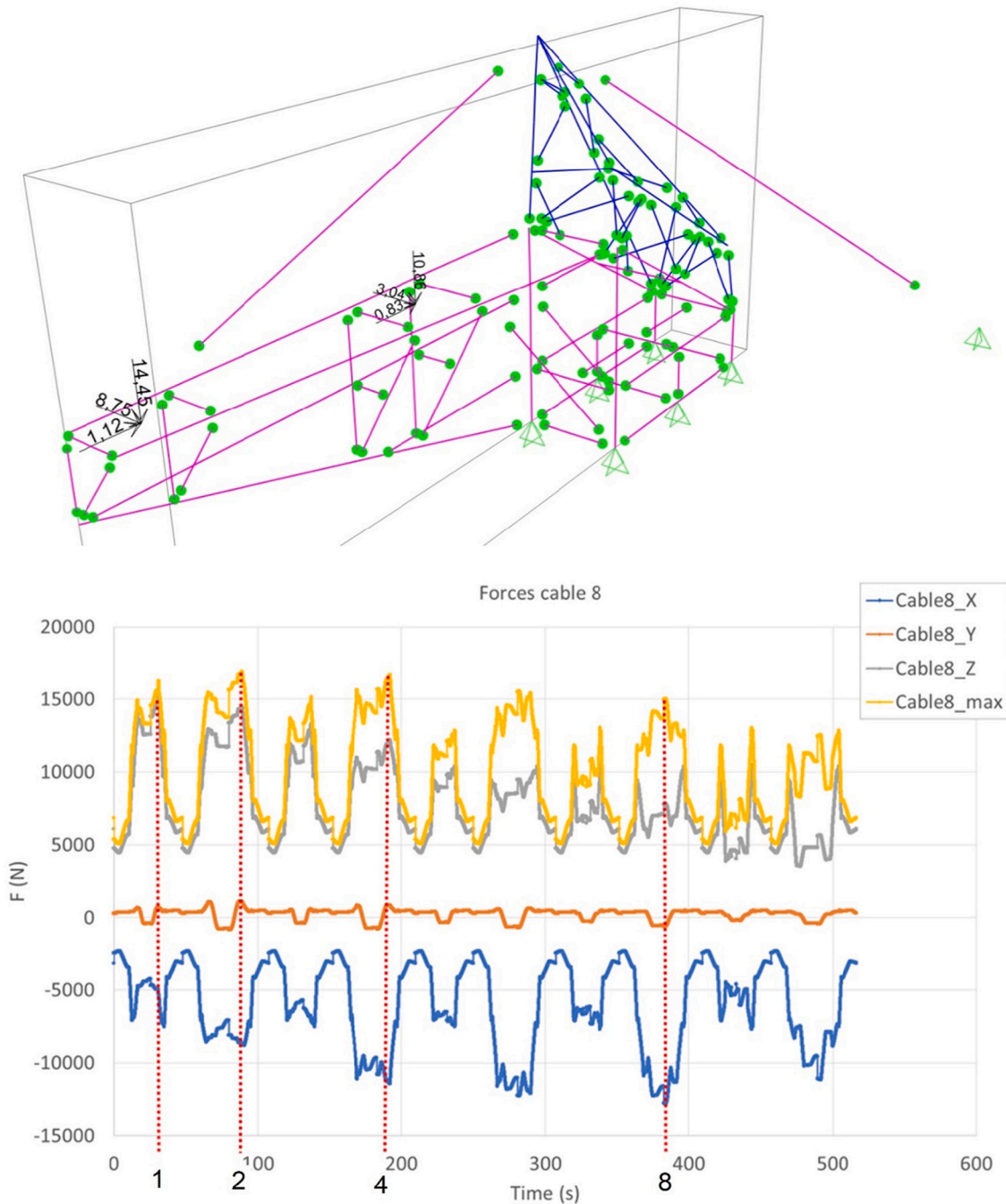
Fig. 9. Inputs for the numerical model of supporting structures. Structures geometry model (left). Cable tensions (right).

workspace, high payloads and modularity that facilitated transportation. This paper presents details on the design, construction and experimental validation of a robotic system using a CDPR for the installation of CWMs in a real environment. To the best of the authors' knowledge, the present paper represents the first study and development thoroughly addressing such an application. The main research focus relied on the following points:

- Question 1: Is the CDPR feasible for the installation of the CWMs with the required accuracy? Within this context, the following sub-questions arise:

o How accurate will the location of the CDPR platform be?
o How accurate will the fine bracket (or connector) positioning be?
o How accurate will the placement of the CWM onto the brackets be?
- Question 2: Will the performance of the CDPR system for the installation of CWMs be more competitive than manual methods in terms of working time?

The remainder of this article serves to clarify these questions and to show the technical developments that were used to solve them. In the second section, the conceptual framework used in this research is explained. In the third section, the prototyping and tests are described.
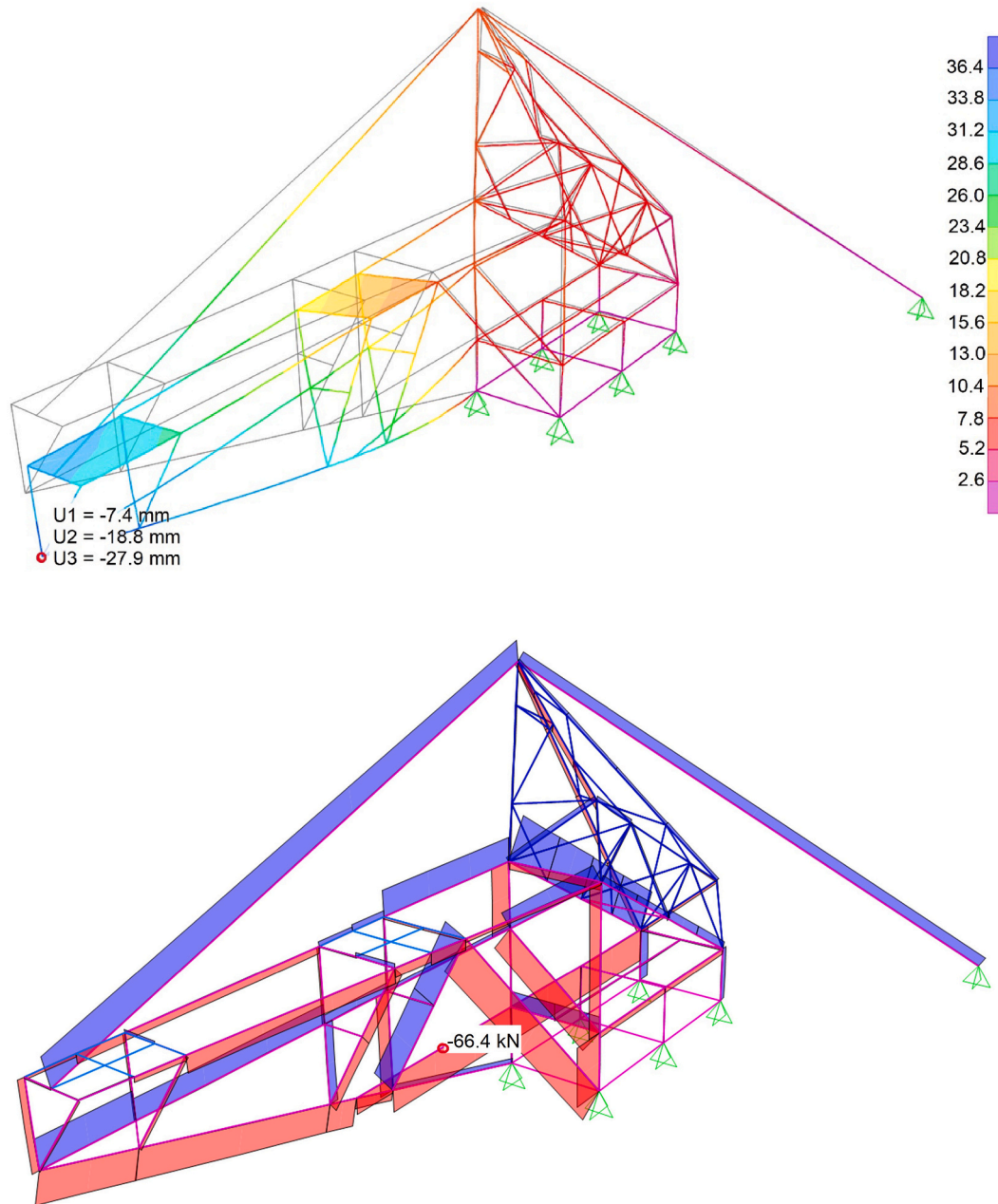
Fig. 10. Results from numerical model of supporting structures. Displacements (left), axial forces (right).

Future needs for possible marketing are defined in the conclusion.

2. Conceptual framework and description of the adopted system

The system used in the Hephaestus project is complex. The field of robotized and automated façade renovation of existing building façades with modules requires a specific context and, for this reason, a novel conceptual framework or method was defined. This conceptual framework was based on matrix-based decision-making methods [38–40] and specific problem-solving methods [41] [42]. The conceptual framework utilized during the different research phases and the topics of each sub-systems evolved according to research gaps, solutions and future needs. The conceptual framework consisted of three sub-systems:

- **Sub-system 1**: a cable-driven parallel robot for the rough positioning. This is explained in Section 2.1.
- **Sub-system 2**: a set of robotic tools named Modular End Effector (MEE) on top of the CDPR for fine positioning. This is explained in Section 2.2.
- **Sub-system 3**: a control system executing the commands and synchronizing the tasks of the CDPR and MEE. This is explained in Section 2.3.

The aforementioned tasks (bracket installation and CWM installation) required high relative and absolute accuracy. To accomplish such accuracy, it was necessary to know the precision of the CDPR, which was estimated to have a positioning tolerance of 40 mm [43]. Therefore,

Fig. 11. Fixing systems of supporting structures to the demonstration building.
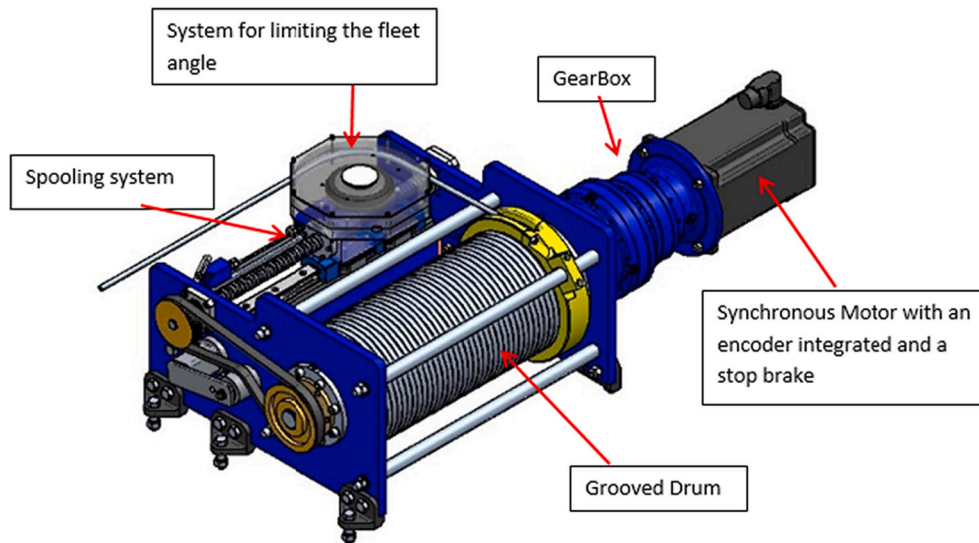
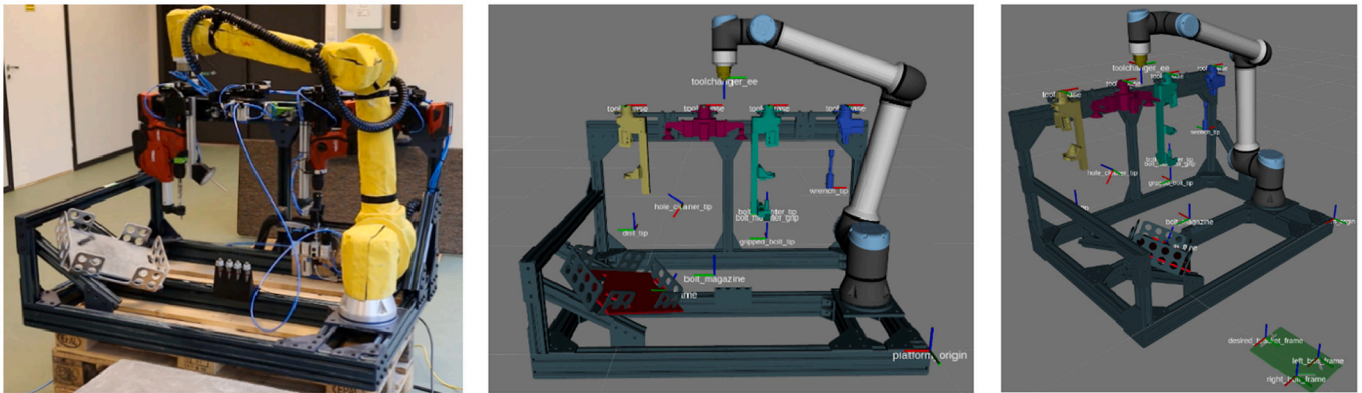**Fig. 12.** CAD view of the VICINAY Winch WB21.L.30S.1.

Fig. 13. Robotic arm and its tools before mounting on the CDPR platform.

during early stages of the project, two means for installing the brackets were foreseen: the CDPR for rough positioning of the platform containing the MEE, and the MEE along with its tools for fine positioning of the brackets. It was decided that the installation of the CWMs onto the brackets would be a semi-automated process that would require manual adjustment.

The CDPR was configured for covering a façade of 8.5 m wide by 10.2 m high where several CWMs could be installed. The system was implemented in two demonstration buildings. During the first demonstration (see Fig. 4), all the devices, hardware and software were implemented, integrated and performed for the first time. During the second demonstration (see Fig. 8), the aforementioned tasks (bracket installation and CWM installation) were completed, proved and measured.

2.1. CDPR: Geometrical design, calculation, performance, and hardware definition

From a geometrical point of view, a CDPR is an association of cables of variable lengths linking a drawing point attached to a base frame and a fixing point attached to the mobile element or platform. The next section addresses the overall methodology applied in the geometrical design of the Hephaestus CDPR prototype.

2.1.1. Geometrical design and calculation

The CDPR used to displace and position the CWMs in the Hephaestus project is depicted in Fig. 4. The figure shows the top and bottom drawing point assemblies (DPA), cable drawing points (dp), attachment points (ap), and winches (w). The first step in the design of the system is the definition of the overall CDPR geometry. The following characteristics shall be determined: (i) number of cables, (ii) position of the drawing points, (iii) geometry of the platform, and (iv) cable configuration. The geometry of the platform (iii) is defined by the relative positions of the attachment points. Clearly, given the drawing point positions and platform geometry, the designer shall define how these two sets of points are connected by the cables. This choice is referred to as the cable configuration (iv).

Many of the previous projects on 6DOF CDPRs focused on the cases involving eight cables (i). This choice yielded CDPRs with large workspace to footprint ratio and symmetry properties [18,19]. Although a greater number of cables may lead to superior performances, it could come at the expense of additional cost and complexity. Based on these well-known results, we chose eight cables for the Hephaestus prototype. The definition of (ii)-(iv) was addressed in the sequel. The geometrical design of the Hephaestus CDPR was based on the following inputs. First, the (a) desired robot workspace was defined based on the position of the CWMs to be installed on the building facade. Second, the possible range of the (b) payload and its relative position with regard to the platform was estimated from a preliminary study of the equipment and tools that

Fully robotic solution

Tool changing:
- 4 different tools
- 5 tool changes

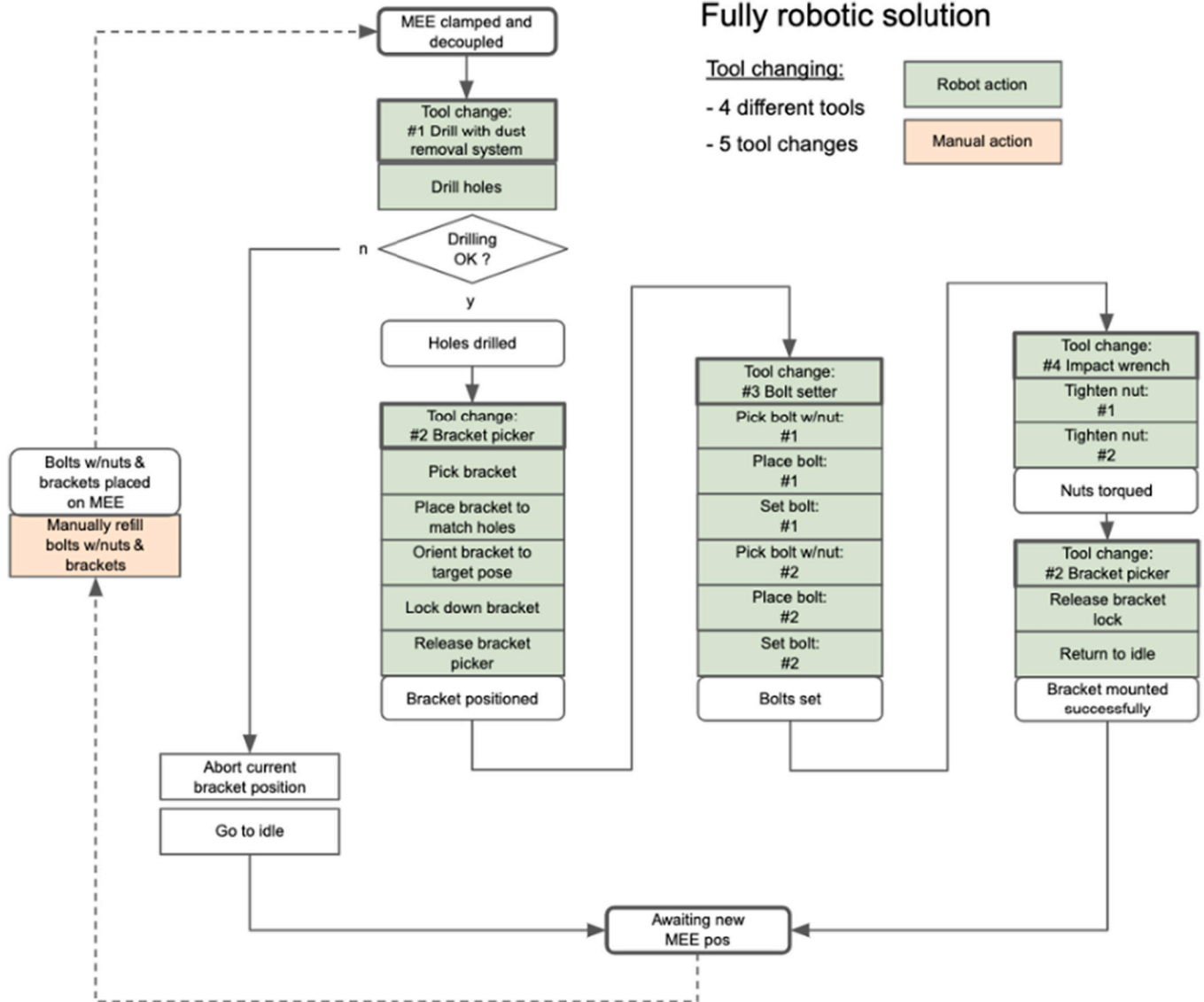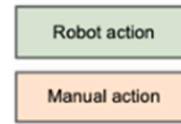| Robot action |

| Manual action |

Fig. 14. Robot arm operation workflow.

should be mounted on the platform. Finally, the (c) necessary positioning precision was defined in order to successfully install the CWMs. Given (ii)–(iv), one might verify whether (a)–(c) could be satisfied through simulations. Furthermore, the Maximum Cable Tension (MCT) necessary to reach poses in the workspace (a) with payloads (b) could be calculated. In particular, this parameter played a crucial role in the mechanical design of the CDPR. The MCT was a key input, for instance, in the design of the winches, pulleys and robot structure. As a result, the cost related to the manufacturing and assembly of a CDPR was strongly related to its MCT. In this context, it was rather reasonable to seek a robot geometry that was able to minimize the MCT across the workspace (a). Accordingly, the design of the Hephaestus CDPR was formulated as an optimization problem, which was to minimize the MCT while taking (ii)–(iv) and (a)–(c) into account. More in detail, the estimation of the MCT using straightforward computational methods may represent a significant computational burden, which can hinder the solution of the proposed optimization problem. The developed approach was designed to overcome this difficulty since it proposed an efficient closed-form expression for the MCT. Further details on the geometrical design of the Hephaestus CDPR can be found in [44].

2.1.2. Performance assessment through simulations

Once the configuration was defined, the performance of the CDPR was validated using three criteria:

- Workspace (based on the CDPR needed to access pick-and-place points for the CWM);
- Wrench capability (based on the CDPR needed to be able to carry the designated loads);
- Wind resistance (based on the CDPR needed to be able to withstand horizontal forces).

Considering the final configuration of the CDPR and the final design of the MEE, it was verified that the working volume of CDPR allowed it to perform different tasks to install CWMs on the façade of the second demonstration building. The rotations that were checked during the configuration phase were ±2 degree around Z axis (vertical axis) along the building surface and + 0/−10 degree around X axis (horizontal axis) in the picking position, where the x,y,z, axes are defined as in Fig. 4. The wrench feasible translational workspace (WFTW) was the space enclosing the positions with no rotation in which the resulting wrench from gravity, in addition to the wrench from any wind forces up to 500
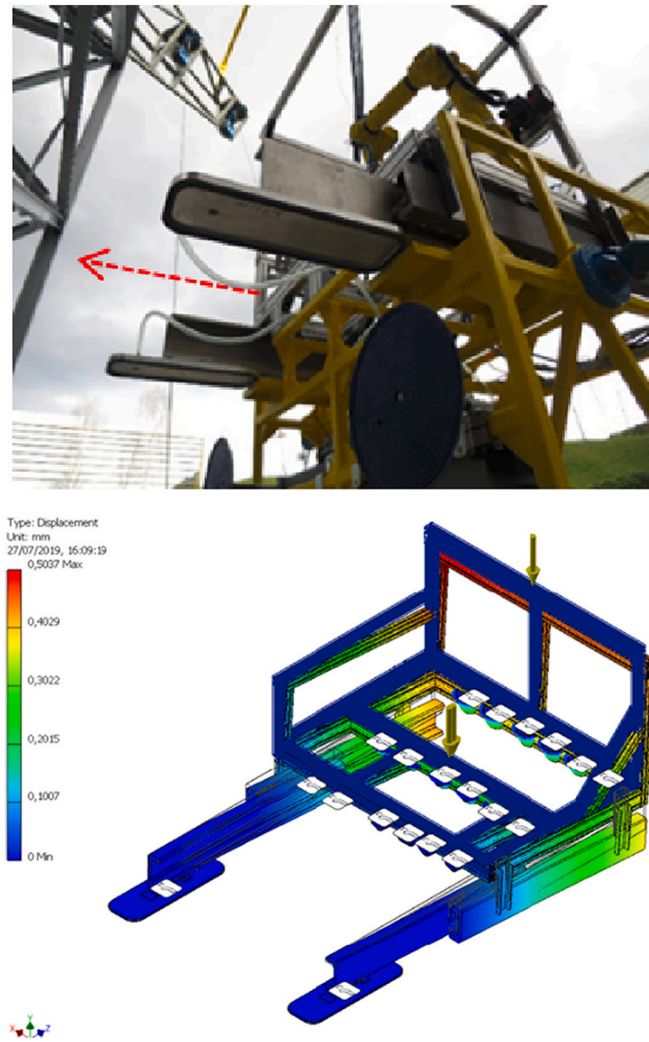
Fig. 15. Stabilizer of the robot's frame prototype during the opening of the stabilizers (top), FEM with the support of the dampers (bottom).

N, could be balanced by cable forces within an acceptable range. This acceptable range was set to be limited by two values:

- On the upper bound, τ_{max};
- On the lower bound, for each cable, $\tau_{min} = \frac{5\rho g L^2}{L_H}$, where
  - o ρg is the weight per meter times gravity (9.81 m/s^2);
  - o L is the distance between points A and B;
  - o L_H is the horizontal distance between points A and B.

This value corresponds to five times the lower limit in order that Irvine's simplified sagging model [45] to be valid. In practice this corresponded to a marginally taut cable: the stiffness in the direction of the cable chord is then at least 10% of the stiffness related to the EA factor, which comes from the material choice and the cable construction. The selection of this limit therefore guarantees that each cable participates consequently to the stiffness of the mobile platform.

The demonstration buildings, and more precisely, their workspaces were defined with three floors, and as mentioned before, with a total height 10.2 m and a width of 8.5 m. The WFTW was built through cuts at various Y coordinates. Considering that the CWM was out of the building when X coordinate of the platform center was 3.5 m, and that in any case cable 2 or 7 would collide with the platform when X reached more than 4.15 m in absolute value, the workspace was truncated at X = ±3.5 m. For a given Y coordinate, the Z limit is taken as the smallest workspace limit obtained for all. Table 1 shows the limit coordinates of the WFTW applied throughout X axis from −3.5 m to 3.5 m. The WFTW can be represented as a series of parallelepipeds calculated at each Y cut. For several values of Y, Z limits are calculated.

The wrench capability was defined as the set of wrenches (a set in the 6D space of forces and torques) that could be balanced by the CDPR in a prescribed workspace. The main interest in this part of the study resided in the wrenches due to gravity, in particular the torques around the horizontal axes which may lead to the platform tipping. The capabilities in three of the components of the wrenches were observed: the force along Z (from the gravity), and the torques around X and Y related to the position of the Center of Mass (CoM) relative to the mobile platform geometric center (reference point).

The result of the study was a set of polygons of stability, which are the loci in XY platform coordinates for the CoM at which the platform will be stable within the designated workspace. Each polygon was computed for a different value of the load applied on the platform, while considering (in this stage of calculation) a wind force of up to 500 N coming from any horizontal direction. Each polygon was computed for a different value of the load applied on the platform. The platform was considered stable in the designated workspace as long as its CoM was within the polygon of stability of the corresponding weight. These polygons were valid for a wind force of up to 500 N coming from any direction. Fig. 5 shows a set of polygons of stability for different values of
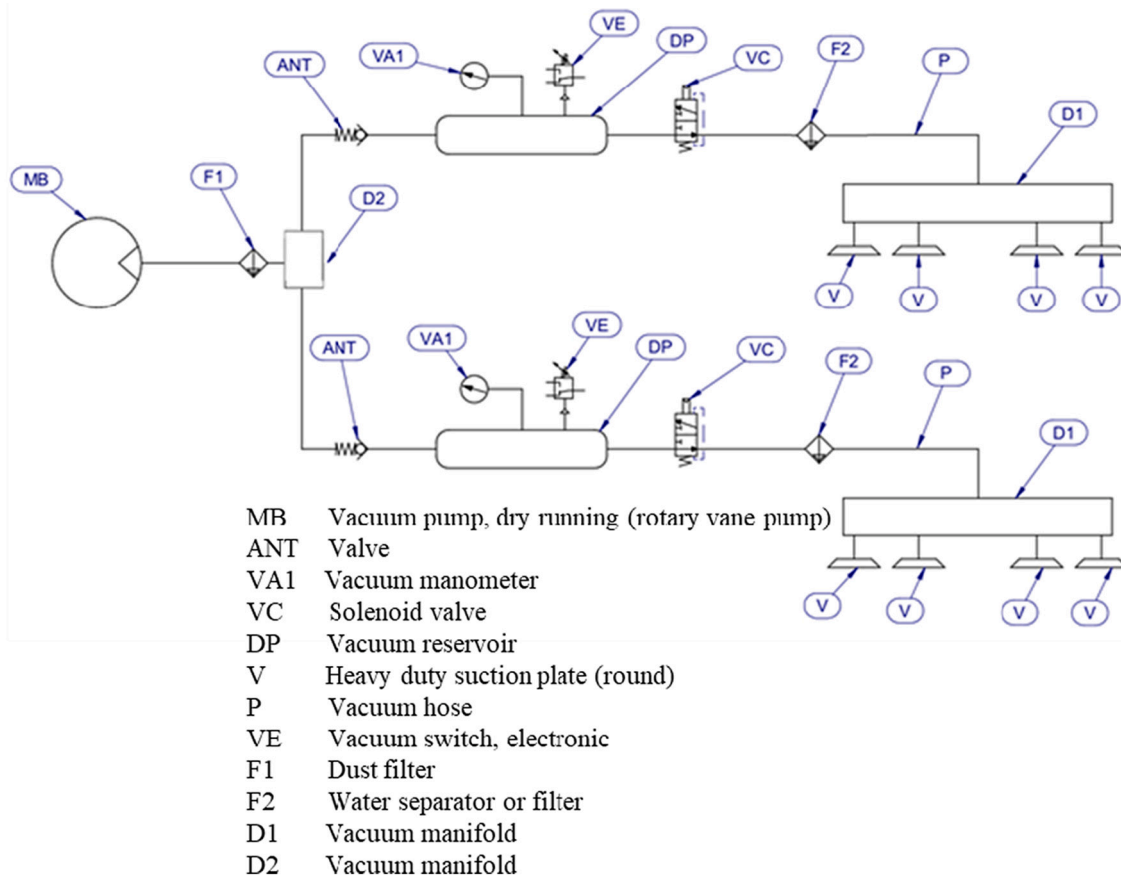
MB	Vacuum pump, dry running (rotary vane pump)
ANT	Valve
VA1	Vacuum manometer
VC	Solenoid valve
DP	Vacuum reservoir
V	Heavy duty suction plate (round)
P	Vacuum hose
VE	Vacuum switch, electronic
F1	Dust filter
F2	Water separator or filter
D1	Vacuum manifold
D2	Vacuum manifold

Fig. 16. Scheme of the VLS.

the load, from 690 kg to 1000 kg, considering the reference workspace described in Fig. 7. They are shown in relationship with the dimensions of the platform in the same reference frame (in yellow) and of the CWM (in blue). Green line represents the objective of performance set during the Geometric Design phase. (See Fig. 6.)

For each polygon of stability, a barycenter could be found. It corresponded to the weighted sum of all points of the polygon, weighted by the sum of lengths of the segments around it, and divided by twice the perimeter of the polygon. This barycenter was the farthest point from all segments. In this study, if the CoM was coincident with the barycenter, it therefore meant that the platform was the most stable, indicating that it resisted better external wrenches.

The CoM position has been estimated through weighing of the actual components using the nominal positions of these components and their own CoM as calculated through CAD. It was right above the barycenter of the polygon of stability of the matching load (1000 kg). For lighter loads, the barycenter was further towards the face where the CWM was loaded. A lighter platform should therefore be loaded even further from the center of the platform, close to the CWM loading position. Next, the analysis and definition of the trajectories of the CDPR to perform the different tasks for the assembly of CWMs were performed. The typical trajectory of the CDPR was the CWM installation trajectory. It consisted of the sequences of picking and placing each of the 10 panels, starting with the first row and then completing the second row. The load configuration in that situation was CDPR carrying the MEE unloaded and the CWM on the way in, and only the MEE on the way back. The maximum Cartesian speed was defined overall, with different values in function of the steps: 10 m/min at low-speed steps and 30 m/min at high-speed steps. The behavior of the robot was simulated along the trajectory shown in the following figures. The trajectory represented the mounting of several CWMs onto the building façade. In Fig. 7, the

workspace of the CDPR is visualized in red. It can be observed that the trajectory lies mostly within the workspace, but the upper mounting positions are at the border of the workspace.

2.1.3. Hardware definition

With the aforementioned input, the mechanical and electrical design of the CDPR was performed. The CDPR comprised the following components:

- The supporting structures corresponding to each DPA, which were designed in order to transfer the load from the swivel pulleys and the winches to the anchoring elements.
- A mobile platform moved by the cable system hosting different tools of the MEE. The total weight of the fully loaded platform reached 1460 kg, of which 350 kg accounted for the carried CWM. It featured the eight fixing points placed according to the dimensions that were defined in the geometrical design, as well as the various tools and power systems for the MEE.
- Eight cables and the corresponding winches. The winches were used to control the length of the cables and the cable tensions.
- Cable routing elements: Pulleys (i.e., sheaves) were used to route the cables from the winch to the mobile platform; Force sensors were placed at one of the routing pulleys of each DPA to measure the cable tensions.
- Power and data feeding cables to the platform.
- Electrical cabinet containing the power (e.g., drive, amplifier, converter, etc.) and control (e.g., computer, fieldbus interface, etc.) required for the winch motors. This was a weatherproof electrical cabinet housing the central control unit. It featured the servomotor drives, the associated power units, the central programmable logic
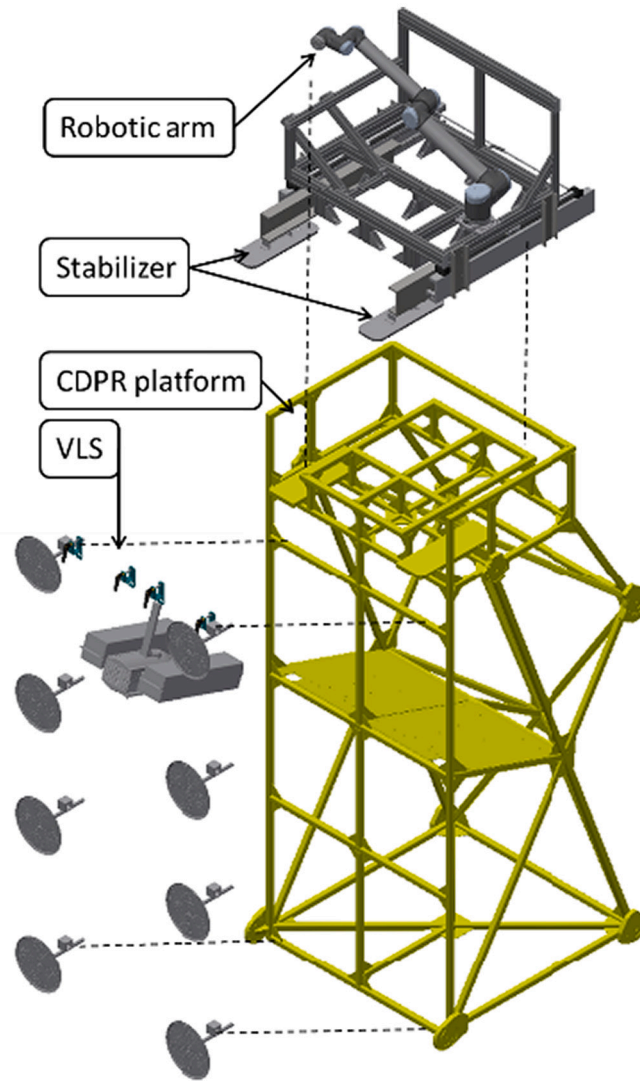
Fig. 17. View of the MEE on top of the CDPR platform during the first demonstrator (top), exploded view of the front side (bottom).

controller (PLC) where the central control was implemented, and the associated inputs/outputs acquisition system.

- A control room where the master computer and the operator(s) responsible for the safety and proper operation of the CDPR were located.
- A rack where the CWMs (or other type of prefabricated modules) were stored for pick up by the MEE attached to the CDPR.

A 3D CAD view of the design of the whole Hephaestus CDPR system can be seen in Fig. 8:

2.1.4. Supporting structures of the DPAs

The structure of a CDPR secures the winches and pulleys in place and transmits the forces from the cables to the ground. In the Hephaestus project, the supporting structures were composed of six independent welded-steel structural elements. The supporting structures were designed considering the locations of the drawing points A_i (i.e., last contact point between the pulley and the cable), the cable routing elements (i.e., pulleys) and the winches. Each upper supporting structure was designed to hold two winches, two drawing points and two cable routing elements. Each lower supporting structure held just one winch, one A_i point and one cable routing element. In order to fulfill the design criteria of "easy to be assembled and set up on site," the supporting

structures, winches and cable routing elements were mounted on a laboratory where the assembly tolerances could be assessed and then transported to the control office on site. The supporting structure was optimized by a FEM analysis in which the following inputs were considered:

- Coordinates (X, Y, Z) of the drawing points in accordance with the geometrical design.
- Maximum force applied by the cables (and its direction): It was assumed based on the forces in three directions (X, Y and Z) at each A_i point (drawing points): F_x (horizontal force parallel to the building façade); F_y (horizontal force perpendicular to the building façade); and F_z (vertical load). From these values, the resultant force F result applied at each A_i point was computed, as well as the direction of the resultant force.
- Maximum displacement tolerances (in three directions X, Y, Z) of the cable drawing points. The admissible displacement was defined as 50 mm (note that the displacement tolerances include construction tolerances).
- Time-history evolution of tensile forces applied by the cables at each drawing point A_i during the whole CWM installation process of covering the second demonstration building façade was obtained from CDPR simulations (Fig. 10 right).
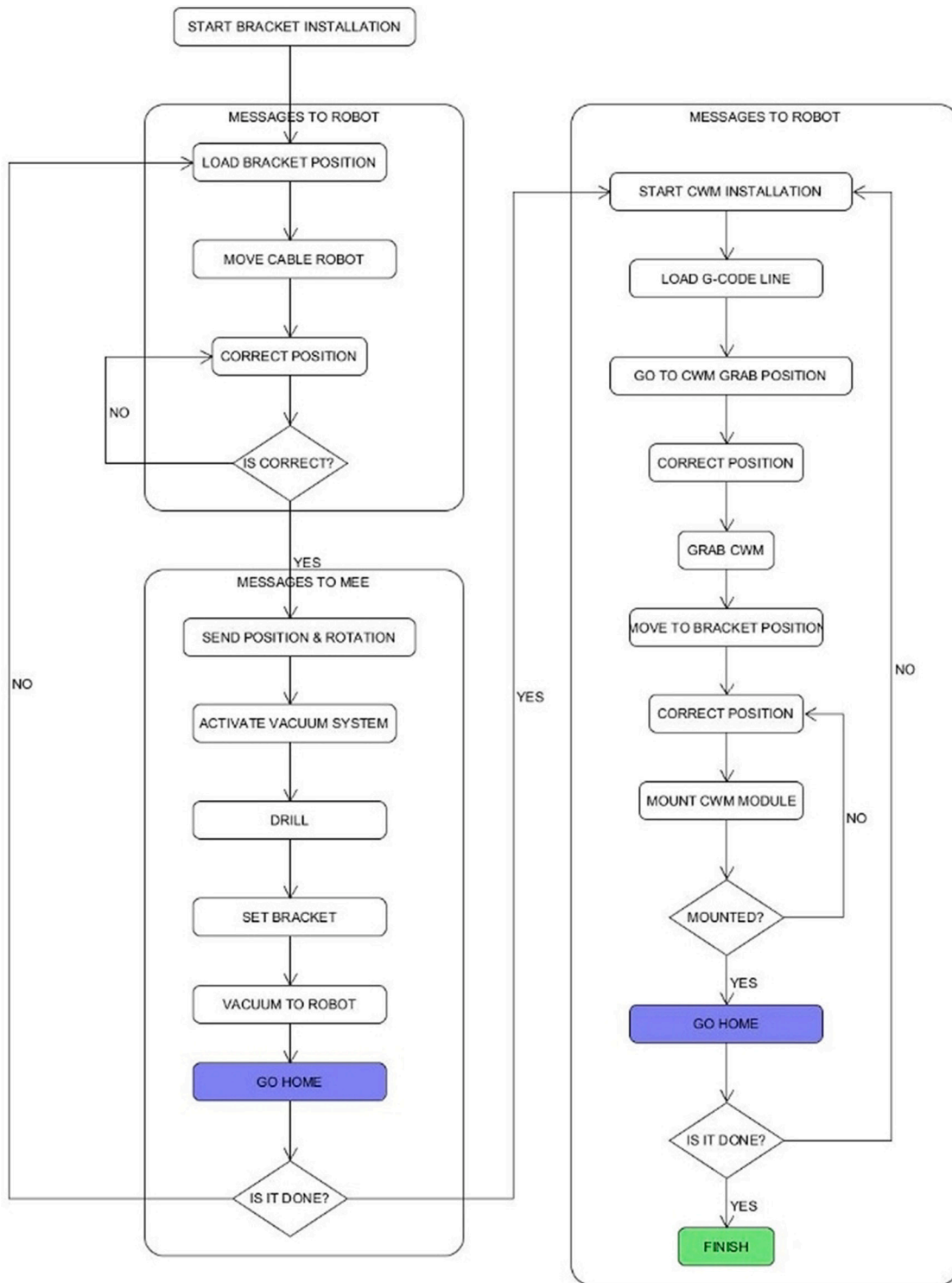
Fig. 18. Bracket installation simplified state machine diagram.

For the Finite Element Method (FEM) analysis of the supporting structures, the software SAP2000® [46] was used. The steel profiles of the structures were modeled using frame elements, and moment releases were placed in the connections between some profiles to simulate pinned connections (Fig. 9). Only elastic material properties of steel S275 were used, with an elastic modulus of 210 GPa and a Poisson coefficient of 0.30.

These forces varied in time both in magnitude and direction, so they were applied to the model as separated time-history forces in three directions (X, Y and Z).

After the analysis of the model, it was checked that all displacements were below 50 mm, which was the imposed admissible tolerance limit for an adequate performance of the CDPR. Moreover, the von Mises yield criterion in the steel profiles were computed, and it was verified that all of them remained below critical values (Fig. 10), according to structural design recommendations.

Finally, the supporting structures reactions were obtained from the model, and they were used to design the fixing systems of these

Fig. 19. A step-by-step algorithm ensures the status of the main controllers.

structures to the demonstration buildings. Regarding the top supporting structures, steel anchorage plates embedded in the concrete slab on the third floor were designed (Fig. 11), while the bottom supporting structure's chemical anchors with steel rods were used for the connection to concrete foundations (Fig. 11). These reactions were also used for the design of the demonstration building.
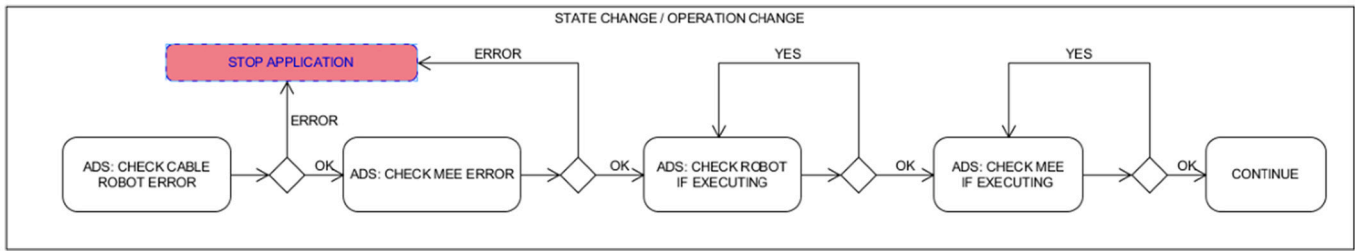
2.1.5. Winches

Each drawing point needs a winch, a swivel pulley at the location of the drawing point, and a force sensor for monitoring the cable tension. The components are the same for all drawing points. The traveling sheave winches (VICINAY winches WB21.L30S.1: SWL 15.7 kN, drum torque 2128 Nm, velocity 30 m/min, cable travel 16 m, see winch in Figs. 4 and 12) were powered by a servomotor with a brake and an absolute integrated multi-turn encoder, associated to a gearbox and wire rope spooling mechanism synchronized with the grooved drum. The swivel pulley installed at the theoretical location of the drawing point rotated around a vertical axis; it guided the cable towards the attachment point in the mobile platform. The force sensor was embedded in the shaft of the fixed sheave reeving system, directing the cable from the winch to the swivel pulley. The steel wire rope was a Ø11mm non-rotating cable with a minimum breaking load of 115.5 kN. (See Fig. 13.)

The standards applied during the development process were EN 14492 [47], EN 13001 [48], ISO 4301 [49], ISO 16625 [50], FEM 1.001 [51], and EN 12385-4 [52]. All elements were designed with safety factors to match the requirements of at least the M5 mechanism group and the cable in M6 with 6.8 safety coefficient. The electrical cables connected to the mobile platform were directed to it by means of a cable chain mechanism fixed to a beam installed between the two top DPAs (see Fig. 4).

2.2. MEE: Robotic arm, stabilizer, and VLS

The MEE was the set of tools performing all the necessary activities for installing the CWM onto the structure of the building. The MEE was fixed to the CDPR platform. In the context of the Hephaestus project, two main activities needed to be performed. First was the fixation of the brackets onto the concrete slabs which was achieved by a robotic arm. Second was the placement of the CWM modules onto the brackets which was achieved by a vacuum lifting system (VLS) attached to the CDPR platform to pick up the CWM from an inclined magazine, place it onto the installed brackets, and release it.

2.2.1. Robotic arm and its tools

Selected tools needed to be manipulated by the robot in order to mount the brackets for holding the CWM to the building. The most versatile method was in-situ mounting and this was the chosen approach in this project. The list of actions needed to be handled by the robotic arm was concluded: drilling holes for anchor bolts, picking up and placing bracket over holes, picking up and placing anchor bolts in holes,

setting bolts into holes, and tightening anchor bolt nuts to pre-set torque. A Universal Robots UR10 [53] was selected as the tool manipulator. This was decided based on previous experience with this robot and its possibilities and limitations, specifically regarding drilling in concrete. The robotic arm also allowed for excellent adaptability to changes based on ongoing project learnings. The arm was mounted on a custom structure made of profiled aluminum bars. A tool-changing system was integrated to give the robotic arm the possibility of manipulating a variety of tools. Four tools were put together to achieve the needed customized functionality: 1) the drilling tool, 2) the bracket picker and holder, 3) the setting tool with a hammer function, and 4) the tool to torque the nut of the anchor. The cycle was completed by returning the bracket holder.

Since the arm was collaborative, one specific limitation was the modest maximum force it was able to apply (e.g. in the drilling sequence). However, by applying software to monitor the forces while drilling, this arm could be programmed to detect when the drill hits a rebar and then automatically adjust the hole and anchor position to avoid collision. Therefore, a collaborative arm with higher sensitivity was used constructively to achieve robust bracket mounting. The robot arm operation workflow is shown in Fig. 14.

2.2.2. Passive stabilizer of the robot's frame

There are previous experiences with a robotic arm on top of a CDPR platform, however, the activities were not performed outdoors (with wind and rain), but in a controlled environment [54]. In the case of Hephaestus, one of the issues regarding the accuracy of the robotic arm relied on the stability of the frame hosting the robotic arm and its tools while performing tasks exposed to outdoor hazards such as wind-load.

To ensure such stability, a linear system with vacuum cups was designed, tested and prototyped. This linear system was conceived for hosting forces of up to 1500 N and was modeled by using FEM analysis (see Fig. 15). The linear system consisted of two subsystems: the linear actuators and the machined steel profiles (see Fig. 15) that run along the rails with the help of carriers.

2.2.3. Vacuum lifting system (VLS) for picking up and placing the CWM

The VLS was capable for picking up and placing the CWM of 350 kg during operations with inclined plans. The VLS was designed to grip, in vertical position, a CWM of the aforementioned mass, with a smooth glass surface, and a surface A_{zx} of 5.1m². The CWM was considered as a parallelepiped with three different faces A (A_{yz}, A_{zx}, A_{xy}) perpendicular to x, y, z axes with values $A = (0.68\ 5.1\ 0.3)^T m^2$ and showing a maximum aerodynamic coefficient c_a at 1.32. It was possible to work in both dry and wet states, without ice, with an estimated friction coefficient of 0.2 (μ in Eq. (3)). The VLS was dimensioned to lift a load greater than or equal to twice its design load with the minimum relative vacuum pressure q_r. Finally, the altitude was considered to be 900 m above sea level, the temperature between −5 to 40°C, and accordingly the wind pressure q_w during service was estimated lower than 125N/m² and the
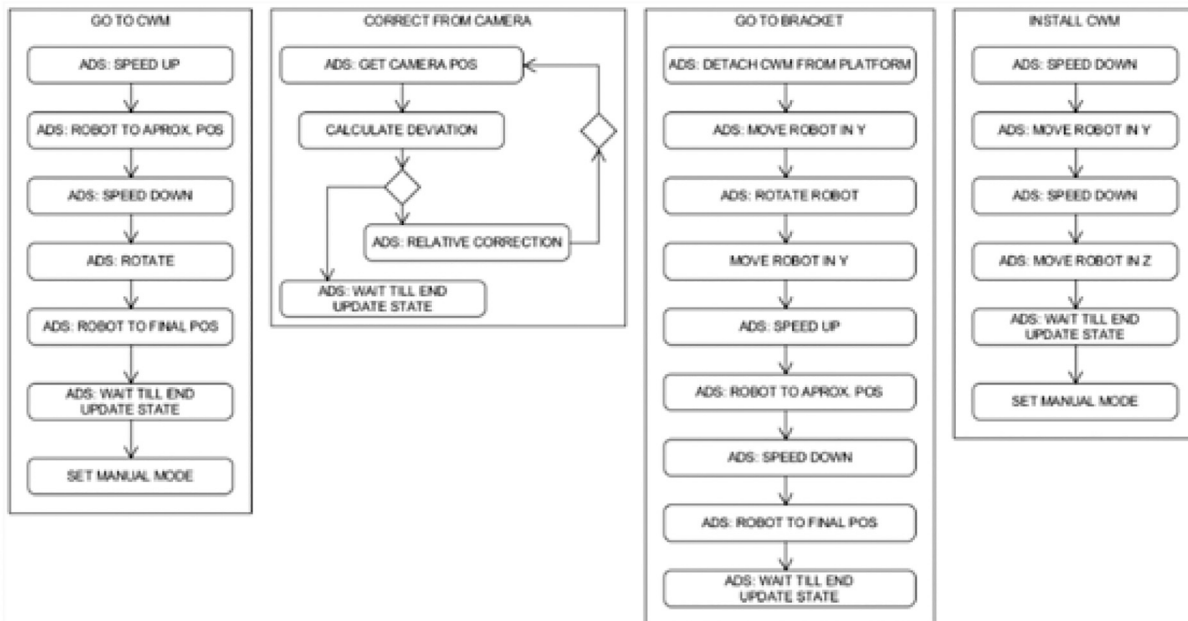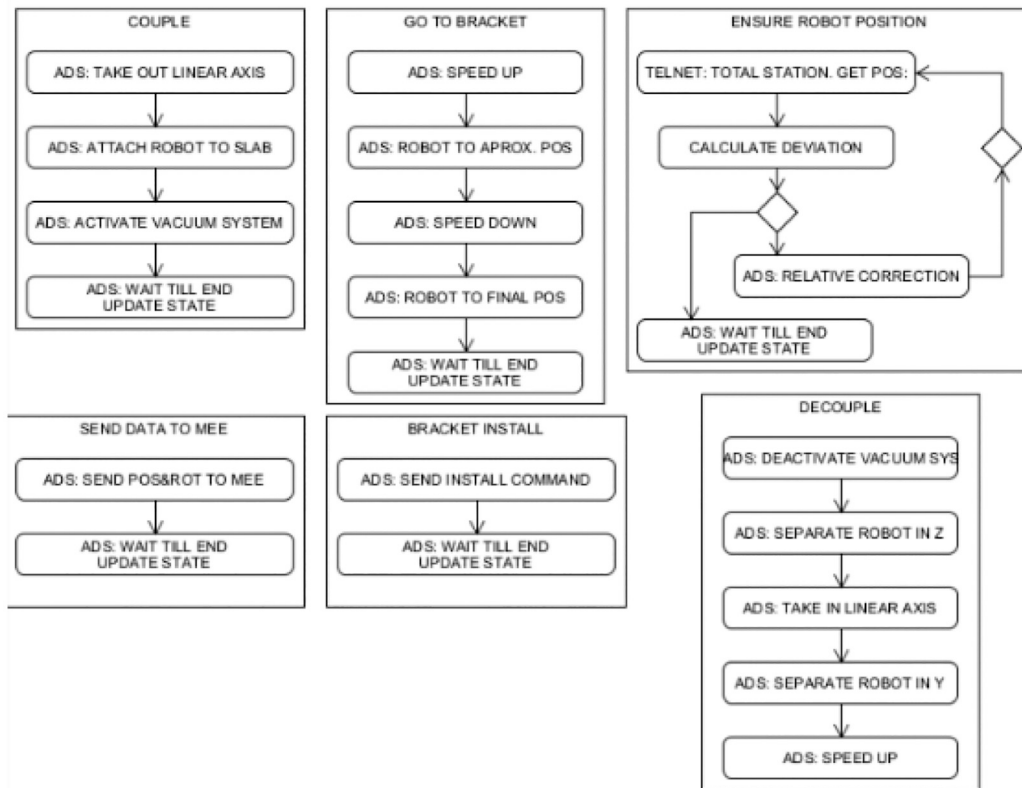
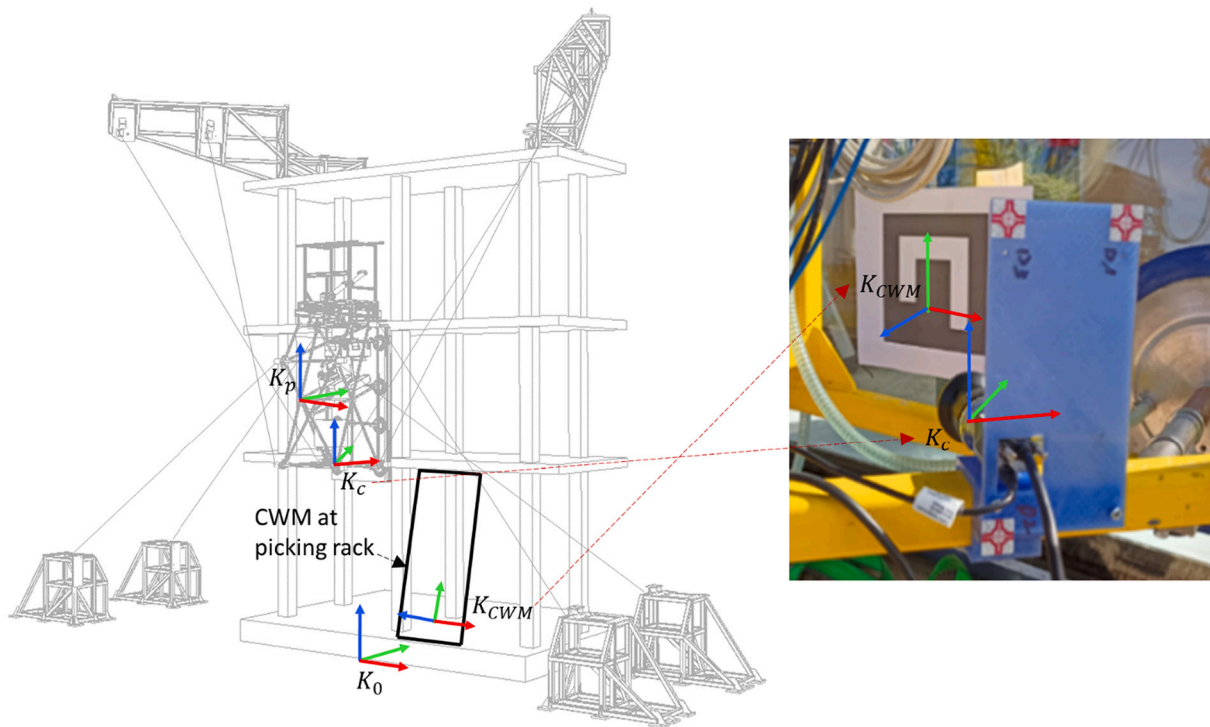**Fig. 20.** Bracket installation and CWM installation simplified states.

Fig. 21. Coordinate systems of the building, the CDPR platform and the location of the CWM.

vacuum differential pressure q_r at least equal to 600 mbar. The system creates a grip force f_g between the surfaces of the CWM and those of the $n = 8$ suction cups, showing a diameter d of Ø360 mm. The total load solicitation vector s was the sum of: the CWM mass m multiplied by gravity vector g, and by acceleration $j = (1\ 1\ 1)$ m/s^2 due to the movement, and the forces due to the wind action f_w, each factored by the applicable partial safety coefficients ($\gamma_p = 1.1$), which are expressed as follows:

$$f_g = n\frac{\pi \bullet d^2 \bullet q_r}{4} = 48.86\ kN \tag{1}$$

$$f_w = c_a \bullet q_w A = (\ 112 \quad 841 \quad 50\ )^T N \tag{2}$$

$$s = \left(\frac{m(g+j)}{\mu \bullet (1\ 1\ 1)^T} + \frac{\gamma_p \bullet f_w}{(\mu \quad 1 \quad \mu)^T}\right) = \begin{pmatrix} 2.52 \\ 2.52 \\ 20.8 \end{pmatrix} kN \tag{3}$$

The current VLS design was validated by f_g being greater than twice any component of s. The VLS, along with its warnings and safety measures are connected to the Beckhoff control and therefore it could be activated automatically as explained in the next section. The hardware used to construct the VLS is shown in Fig. 16:

By combining all the aforementioned descriptions, the set of tools of the MEE was constructed and integrated on top of the CDPR platform as shown in Fig. 17: (See Fig. 18.)

2.3. Control system: State machine, pose adjustment and controlling hardware

The first task regarding the control system was to define the state machine. There were two main operations that the robot should perform in order to complete the CWM installation successfully: first drilling and installing the brackets in the correct positions, then placing the CWMs in the corresponding brackets. Both were launched separately from the main UI, and for each a state machine pattern was implemented and a main state machine created respectively, each of which was linked to several controllers (e.g., CDPR controller, MEE controller and Total Station controller).

Although each state had its own implementation, every step taken from state to state was ensured to check the CDPR and MEE controller's status for the errors or the running mode. Therefore, a step-by-step algorithm (see Fig. 19) was designed to ensure, in a sequential order, that every system was available to continue to the next state. This step-by-step algorithm was also used to wait for different controllers to finish their tasks. (See Fig. 20.)

In each state machine, the required connections were made using ADS protocol for CDPR and MEE controllers, and a TCP/IP telnet connection to link the Total Station. As a result, several classes were programmed that automatized the connection, and any status of the state machine was able to communicate with the different controllers to speed up the robot, activate the vacuum system, take out the linear axis, or any other procedure that must be done in order to complete the operation.

Another topic related to the control system and outlined here is the CDPR platform pose estimation and adjustment. Fig. 21 shows the picking rack that hosted the CWM before being handled by the CDPR platform. The picking rack was supported on both the ground floor foundation and the first-floor slab. The position of the rack was unknown and the location of the CWM on it was not always the same because the CWM weighed approximately 300 kg and was placed by a mobile crane operated manually. For these reasons, the CWM was not placed in a known and repeatable location. Due to aforementioned issues, it was necessary to recognize the CWM and its exact location (translation and rotation) before picking up from the rack and adjusting the pose of the CDPR platform accordingly. Otherwise, the lack of parallelism between the eight vacuum cups of the VLS and the glass in the CWM would result in leaks and, therefore, the vacuum system would not perform correctly.

The pose estimation problem was tackled by using an ArUco Marker [55] on top of the CWM and a camera on the CDPR platform. Vision-based solutions for the calibration of the platform were already developed [56,57], and it was considered useful to implement these in a real outdoor scenario. A single marker of 200 mm by 200 mm was used to

Table 2
Poses, adjustments and deviations.

	Ideal pose	Calculated pose adjustment	Deviation
Tx	2746.86	−0.31	−0.31
Ty	5.47	0.10	0.10
Tz	−2442.42	1.10	1.10
Rx	−5.49	−0.06	−0.06
Ry	0.00	−0.02	−0.02
Rz	−0.41	−0.04	−0.04
Pose 1		Adjustment	Deviation
Tx	2746.86	−3.95	−3.95
Ty	−45.47	42.07	−8.87
Tz	−2442.42	−0.49	−0.49
Rx	−5.49	−0.88	−0.88
Ry	0.00	−0.24	−0.24
Rz	−0.41	0.06	0.06
Pose 2		Adjustment	Deviation
Tx	2746.86	0.48	0.48
Ty	−20.47	18.95	−6.99
Tz	−2442.42	4.60	4.60
Rx	−5.49	−0.17	−0.17
Ry	0.00	−0.12	−0.12
Rz	−0.41	0.32	0.32
Pose 3		Adjustment	Deviation
Tx	2721.86	27.68	2.68
Ty	−20.47	18.89	−7.05
Tz	−2442.42	3.38	3.38
Rx	−5.49	−0.18	−0.18
Ry	0.00	−0.13	−0.13
Rz	−0.41	0.58	0.58
Pose 4		Adjustment	Deviation
Tx	2746.86	6.73	6.79
Ty	−198.13	42.40	−161.20
Tz	−2519.92	−61.03	−138.66
Rx	0.00	−5.21	0.26
Ry	0.00	0.24	0.23
Rz	0.00	0.48	0.91
Pose 5		Adjustment	Deviation
Tx	2746.86	−1.29	−1.29
Ty	−20.47	19.45	−6.49
Tz	−2417.42	−13.11	11.89
Rx	−5.49	0.66	0.66
Ry	0.00	−0.01	−0.01
Rz	−0.41	0.13	0.13

provide correspondences to obtain the camera pose. The inner binary codification made them robust, allowing the possibility of applying error detection and correction techniques. As the central element of the vision system, the camera Basler acA 1920-40 gc [58] was used. The camera contained a Sony IMX249 CMOS sensor and delivered 42 frames per second at 2.35 MP resolution. In addition, the objective [58] was added to the camera. To run the software, the modular computer Nvidia Jetson TX2 [59] was chosen. The software that performed the pose estimation was written in C++ and can be found here [60]. To enable real-time communication with the robot's control unit, the open-source framework ROS [61] was integrated. The main steps enabled by the software were the detection of the ArUco Marker, pose estimation, and processing the information further to the control unit of the robot. For the detection of the marker, the OpenCV library was used [62], which consisted of two main steps. First, an adaptive thresholding to segment the markers was encoded. After the candidate detection, it was necessary to determine if they were actually markers by analyzing their inner codification. For the pose estimation, given the set of 2D point locations and the known physical marker size, the Perspective-n-Point (PnP) algorithm [63] was used to compute the ArUco Marker pose with respect to the camera. The results of the pose estimation were packed in a transformation matrix and published via ROS. The adjustments were computed using the three coordinate frames (see Fig. 21):

- K_0 represented the static coordinate frame of the robot. Movement commands for the platform were expressed in this coordinate system.
- K_p represented the mobile coordinate frame of the platform. The transformation $T_0{}^p$ was given by the platform pose which was calculated by the robot controller.
- K_{CWM} represented the mobile frame of the CWM. The transformation $T_p{}^{CWM}$ was measured by the camera using the OpenCV library.

To calculate the correct adjustment in the form of a transformation matrix *T*, first the ideal relative transformation between the platform and the CWM was recorded $\widehat{T}_p{}^{CWM}$. In the platform coordinate frame, the correct movement can then be calculated to regain this transformation with: $\widehat{T}_p{}^{CWM} \cdot \left(T_p{}^{CWM}\right)^{-1}$. To obtain this movement with respect to the static coordinate frame so that it could be sent to the robot controller, another transformation was added: $T = T_p^0 \cdot \widehat{T}_p{}^{CWM} \cdot \left(T_p{}^{CWM}\right)^{-1} \bullet \left(T_p^0\right)^T$.

This way, a GCode was generated and the adjustment of the CDPR platform could be achieved in a nearly automated mode. The results of this approach were promising but still need further development. As the robot needed to pick up the object, the vision of the camera narrowed as the robot got closer. Therefore, for future research, a valid option might involve integrating various markers to boost the robustness of the results computed by the pose estimation.

In order to examine the accuracy of the test, the ideal pose for picking up the CWM was defined. Apart from that ideal pose, five other poses were defined. Each pose was repeated nine times under similar light conditions and the aforementioned GCode was calculated by using the pose estimation with the camera. Deviations in the ideal pose were calculated as explained in Table 2. With these results, it can be stated that deviations decreased in close ranges and therefore, in future research instances, a multi-pose approximation to the CWM shall be considered before picking it up.

Considering the previous points, the control hardware was set up. In Fig. 22, the scheme of the hardware and wiring of the Hephaestus robot are shown. The system consisted of five PCs in total. The main control unit consisted of two of the PCs: the control PC used to execute a software tool to automate the façade panel installation and the Main Industry PC (IPC) which consisted of a Beckhoff C6650-0050 (See Beckhoff IPC in Main Control Unit in Fig. 22). With the help of a router and a radio module connected to the Beckhoff IPC, the Main Control Unit was able to communicate with all the systems: the Total Station using telnet protocol, the radio controller using WLAN CANopen protocol, and the EtherCAT to communicate with safety sensors, I/Os, force sensors, and drives. (See Fig. 23.)

The Main IPC was also connected to the MEE Control Unit which consisted in a Beckhoff CX130-0155 (See Beckhoff IPC in MEE controlling unit in Fig. 22), through EtherCAT, which was integrated within the EtherCAT network as an EtherCAT slave. Finally the latter was connected to the ROS PC and the camera's embedded PC through Ethernet.

The CDPR controller was based on the TwinCAT 3 software from BECKHOFF [64]. It consisted of a soft PLC and a motion controller (i.e., either a Beckhoff CNC, or an advanced motion controller). On the MEE IPC, a PLC was implemented to control the MEE system made by the ROS-PC to control the UR10Robot, the stabilizer, and the vacuum system.

A main user interface (UI) application controlled the interactions between the user and the main controller. The UI showed the CDPR data such as cable tensions, and which state the robot was performing in real time. It also allowed the user to intercept each state, pause the operation, or stop the task. It was connected to the CDPR controller, allowing the

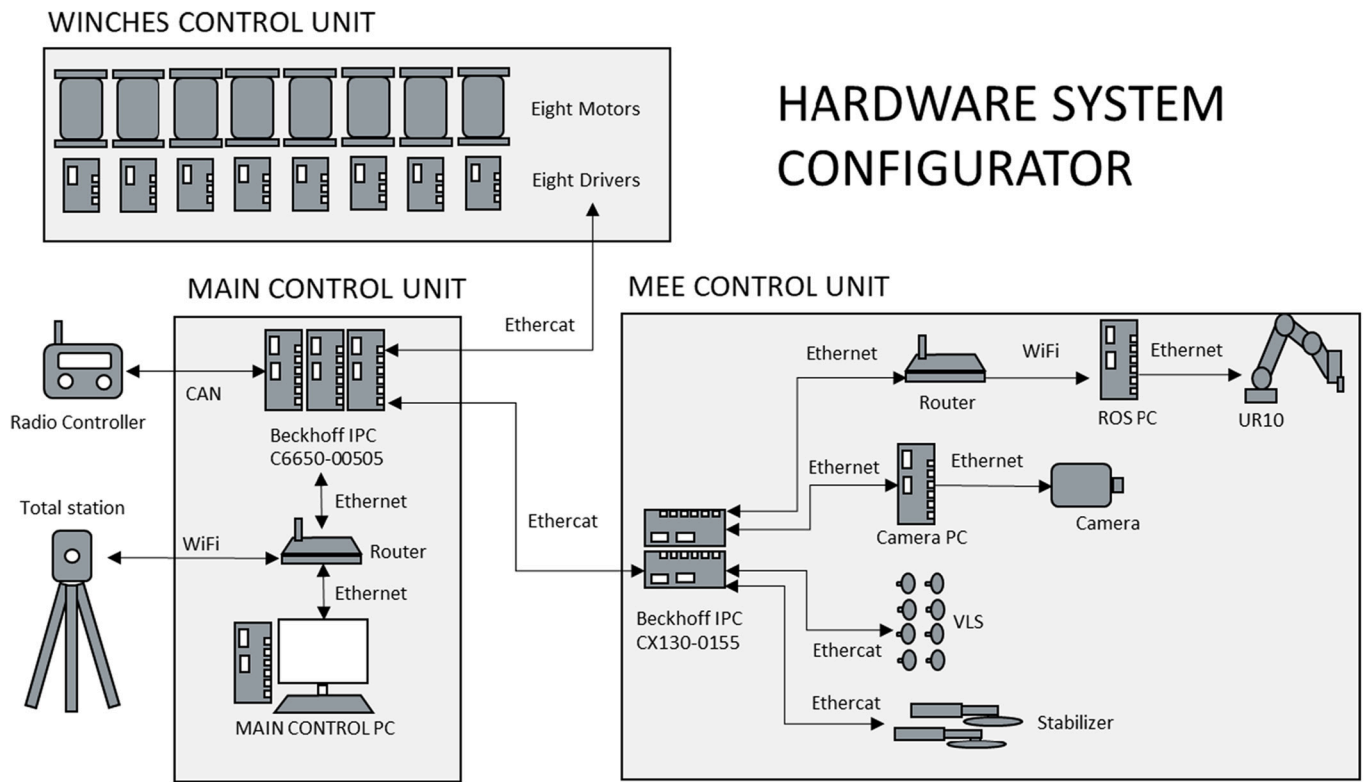**Fig. 22.** Hephaestus wiring layout.

Fig. 23. Fixing supporting structure systems to demonstration building.
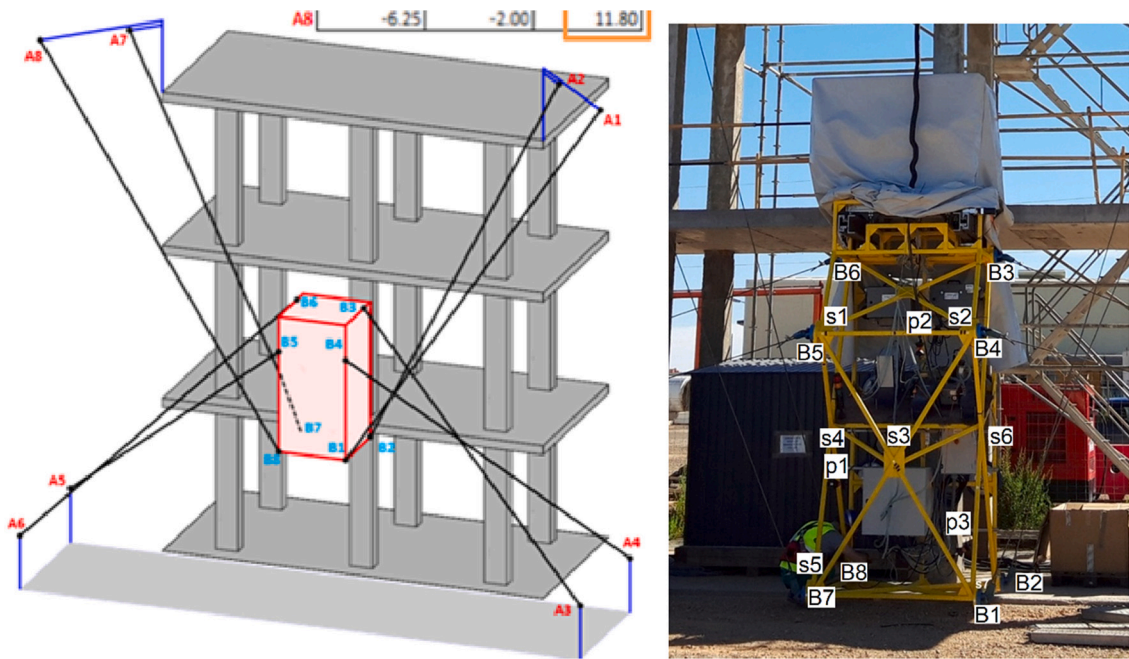
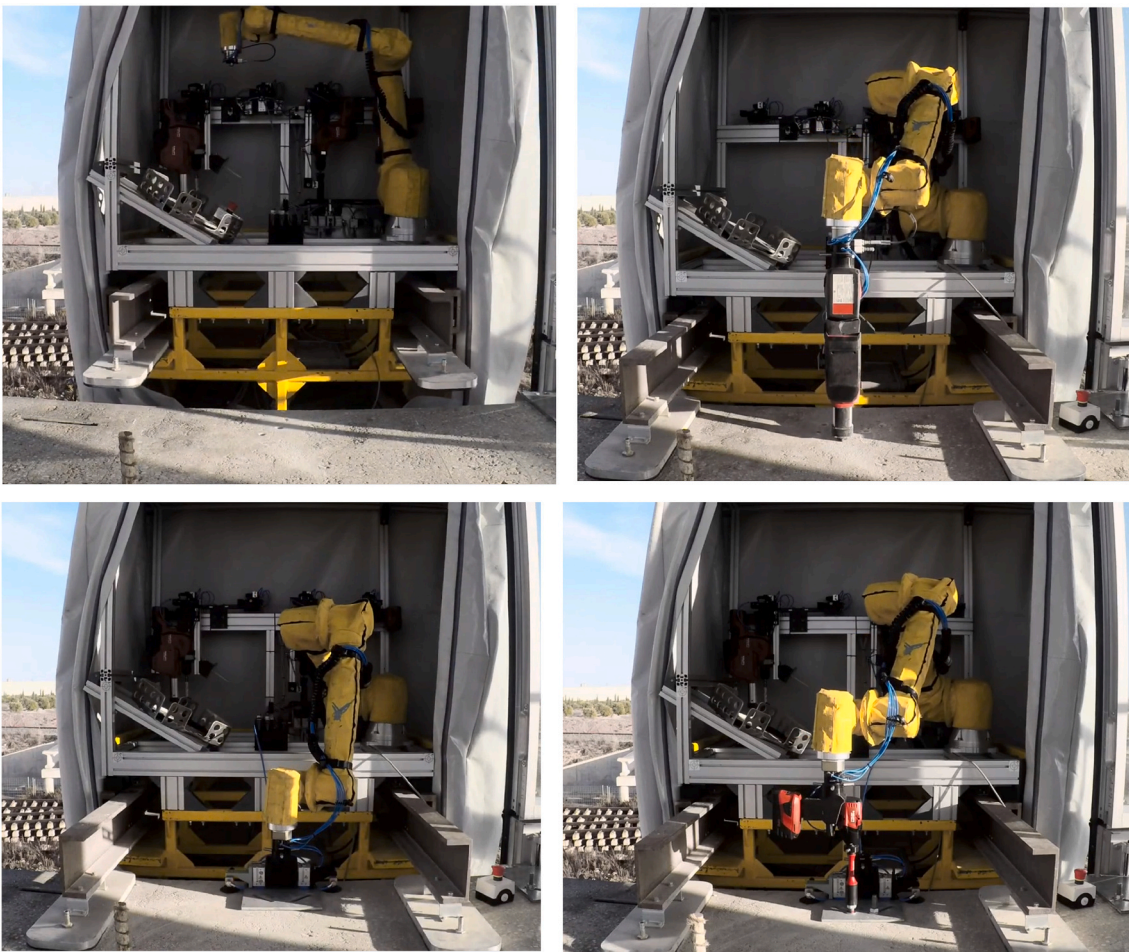**Fig. 24.** Reference points in the mobile platform.

Fig. 25. The MEE in operation during bracket installation [36], see also Video 3.

Table 3
Translation and orientation deviations of the CDPR platform.

|	Translation			Orientation			
PLANNED POSES (m, deg)	X	Y	Z	X°	Y°	Z°	
home	0	0	0	0	0	0	
p0	0	−0.3	0	0	0	0	
p1	−3	−0.3	−2	0	0	0	
p2	−3	−0.3	0.56	0	0	0	
p3	2.4	−0.3	−2	0	0	0	
p4	2.4	−0.3	0.56	0	0	0	
p5	0.7466	−0.3	−1.7879	0	0	−0.5	
p6	0.7466	−0.3	−1.7879	−7	0	−0.5	
p7	0.7466	0.065	−1.7879	−7	0	−0.5	
MEASURED POSES (m, deg)	X	Y	Z	X°	Y°	Z°	
p0	0	−0.292	0	0	0	0	
p1	−2.9928	−0.301	−2.0008	0.0007	−0.2141	−0.2536	
p2	−2.991	−0.2914	0.5589	−0.0217	−0.1524	−0.1089	
p3	2.3919	−0.2974	−1.9958	−0.0223	0.1462	0.4098	
p4	2.3939	−0.2877	0.5589	−0.0443	0.0534	0.0494	
p5	0.7448	−0.2971	−1.7852	0.1762	0.0432	−0.427	
p6	0.747	−0.2802	−1.7978	−6.1652	0.051	−0.579	
p7	0.7449	0.0628	−1.7976	−6.3835	0.0416	−0.3601	
				RESULT – orientation and position errors			
				Orientation errors (deg)			Position error
ERRORS	X	Y	Z	X°	Y°	Z°	
p0	0	0.008	0	0	0	0	0,008
p1	0.0072	−0.001	−0.0008	0.0007	−0.2141	−0.2536	0,0073
p2	0.009	0.0086	−0.0011	−0.0217	−0.1524	−0.1089	0,0125
p3	−0.0081	0.0026	0.0042	−0.0223	0.1462	0.4098	0,0095
p4	−0.0061	0.0123	−0.0011	−0.0443	0.0534	0.0494	0,0138
p5	−0.0018	0.0029	0.0027	0.1762	0.0432	0.073	0,0044
p6	0.0004	0.0198	−0.0099	0.8348	0.051	−0.079	0,0221
p7	−0.0017	−0.0022	−0.0097	0.6165	0.0416	0.1399	0,0101
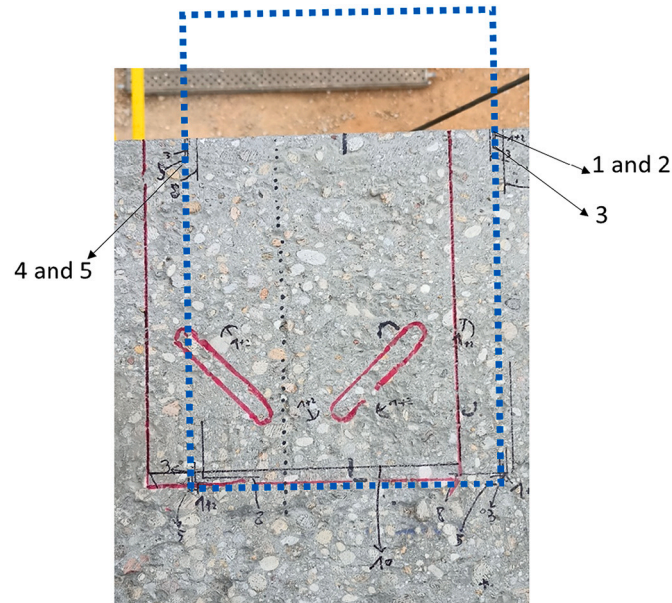
Fig. 26. Bracket placement accuracy and repeatability in different positions.
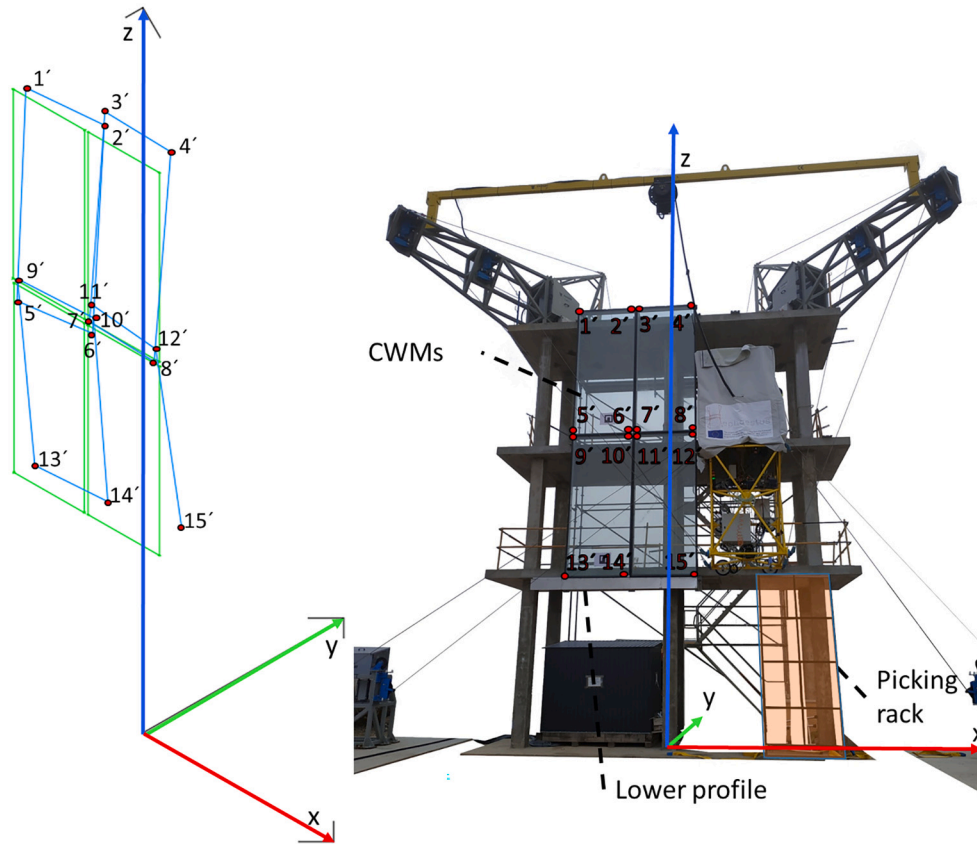
Fig. 27. Measured points' locations.

Table 4
Deviation of the modules in the second demonstration.

Planned point	Xn (mm)	Yn (mm)	Zn (mm)	Placed points	xn′ (mm)	yn′ (mm)	zn′ (mm)	d	d z
1	2304	−295	10,304	1′	−2300	286	10,303	9,90	9,85
2	−870	−295	10,304	2′	−866	−279	10,302	16,61	16,49
3	−804	−295	10,304	3′	−802	−280	10,315	18,71	15,13
4	629	−296	10,304	4′	629	−284	10,316	16,97	12,00
5	−2304	−295	6980	5′	−2294	−301	6968	16,73	11,66
6	−870	−295	6980	6′	−86	−295	6971	12,04	8,00
7	−804	−295	6980	7′	−800	−297	6982	4,90	4,47
8	629	−296	6980	8′	631	−303	6985	8,53	7,03
9	−2291	−295	6907	9′	−2283	−299	6916	12,69	8,94
10	−882	−295	6907	10′	−873	−294	6915	12,08	9,06
11	−804	−295	6904	11′	−799	−297	6926	22,65	5,39
12	629	−296	6904	12′	632	−302	6923	20,15	6,71
13	−2291	−295	3577	13′	−2286	−279	3577	16,76	16,76
14	−882	−295	3577	14′	−879	−274	3577	21,21	21,21
15	629	−296	3580	15	629	−273	3593	26,42	23,00

Table 5
Worker hours for the installation of CDPR workspaces.

Setting up the CDPR workspace	hours	Operators	Total hours
Define the workspace			
Organize the task and define robot workspaces	0.5 h	1	0.5
Transform the coordinates of the brackets	0.5 h	1	0.5 h
Installation of the CDPR			
Install cranes and cables	40 h	3	120 h
Install electrical circuit	8 h	2	16 h
Install platform, including the MEE	2 h	2	4 h
Calibrate the CDPR with regard to the building	4 h	2	8 h
Uninstall the CDPR when tasks are finished	8 h	3	24 h
TOTAL hours			**173 h**

Table 6
Worker hours for a bracket installation.

	Time (hours)
Move the CDPR to the bracket location	0.00833 h
Install one bracket with the MEE	
Open linear actuators	0.025
Move platform downwards and activate the suction cups	
Measure the location MEE by using a Total Station and calibrate	0.05 h
Make holes in concrete	0.0167 h
Pick up, place, and hold the bracket	0.0167 h
Fasten the anchor	0.033 h
Torque the anchor	0.033 h
Release the torque tool	0.00833 h
Release the bracket clamper and leave in the magazine	0.0167 h
Total hours	**0.18 h**

Table 7
Worker hours for CWM installation.

Install the curtain wall	Time	Operators
Place the CWM in the rack	0.0833 h	2
Pick up the Curtain Wall Module.	0.0833 h	
Move the CDPR platform to the magazine		1
Adjust CDPR platform to the CWM		1
Grip the CWM in a desired or known position		
Place curtain wall onto the brackets	0.0833 h	1
Localize the brackets' position.		
Place the CWM onto the brackets		
Total	**0.33 h**	

user to move the CDPR and see what state the CDPR and the MEE were in at any moment. It also allowed the user to operate and control the Total Station controller, allowing the user to obtain position and rotation measurement at will.

3. Prototyping and tests in real environment

The workspaces of the CDPR were similar in the two demonstration buildings and the CDPR hardware remained the same. The bracket installation was performed successfully and the CWM was lifted appropriately. The details are introduced as follows.

3.1. Building structures used for the two demonstration buildings

The first demonstration was performed in Tecnalia facilities in Derio, Basque Country, Spain from October 25, 2019 to January 24, 2020. Once all the components of the demonstrator were installed, the operation of each component (e.g., motors, movement of the robot, positioning in relation with the steel structure, sensor, etc.) was verified. This was the first time the different elements of the robot (winches with cable pulling on the platform/base) and the higher-level control of the robot realizing the coordination of the winches were put together. The steel structure had features to accommodate the top DPAs on the top floor; the bottom DPAs were directly anchored to the ground. The higher platform empty weight was more than expected and the SWL was lower than originally planned (respectively 1110 kg instead of 910 and 15.7 kN instead of 20), which led to the nominal transit positions of the top row of panels being inaccessible. The transit distance for the top floor panels therefore needed to be reduced from 600 mm to 450 mm.

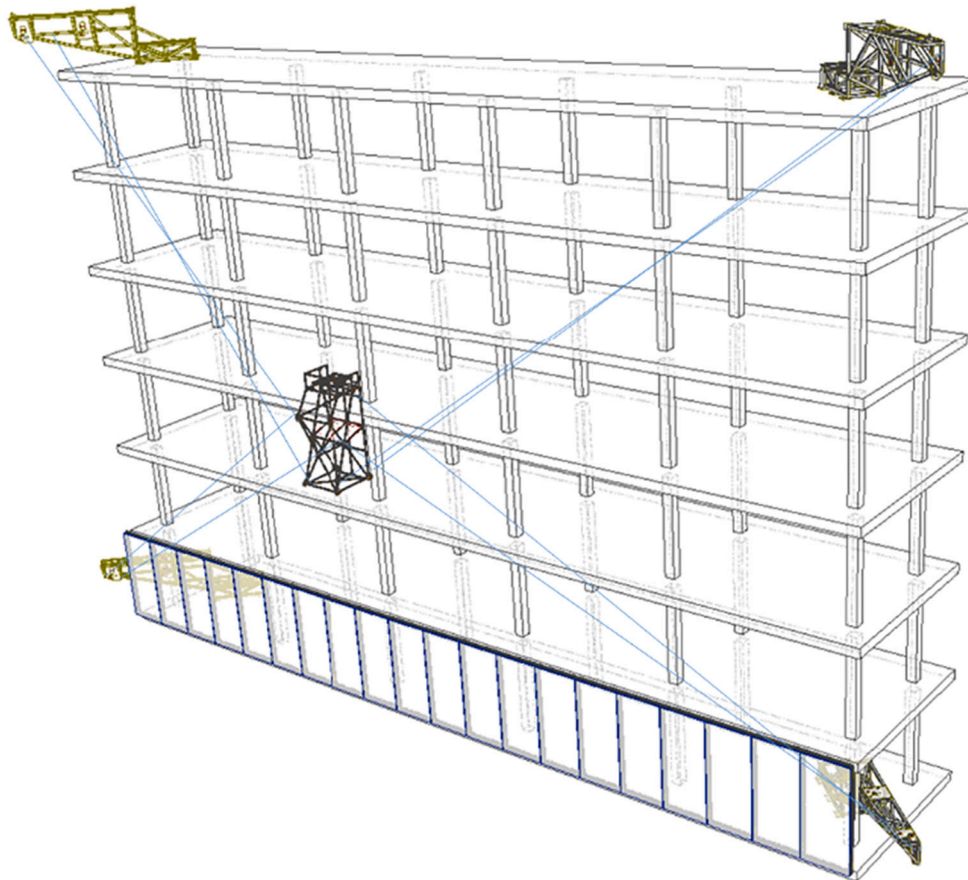The second demonstration took place at Acciona's facilities in

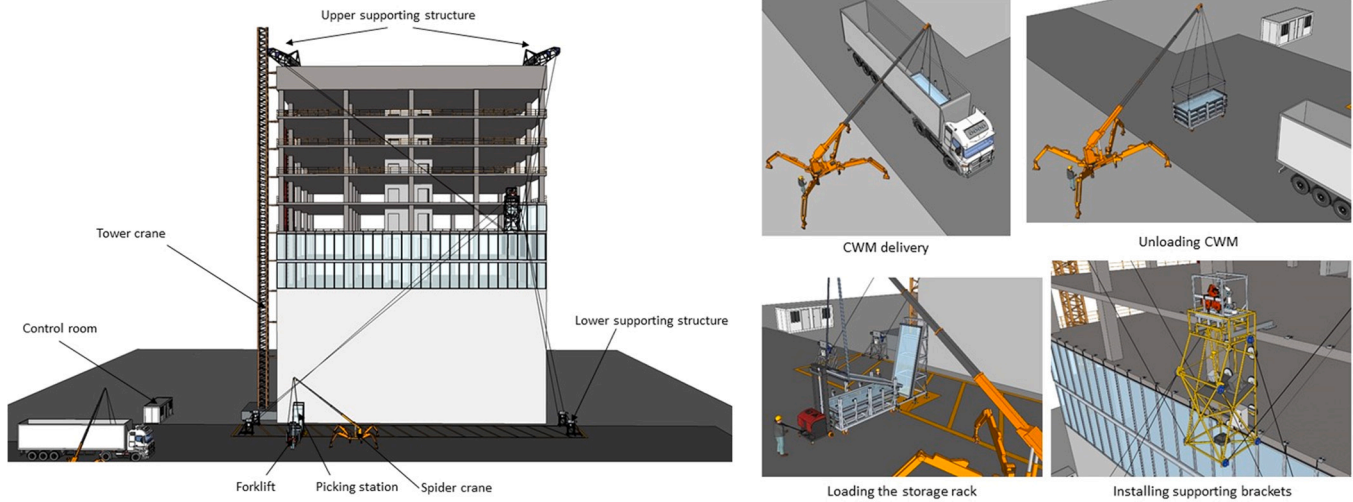**Fig. 28.** Minimum optimal workspace size.

Fig. 29. Future performance of the Hephaestus robot on a construction site.

Noblejas in Castilla-La Mancha, Spain between July 1, 2020 and November 20, 2020. This was the second time the prototype was built, but with more features than that in the first demonstration. In this case, six brackets and four CWMs needed installed. For this purpose, a steel structure was erected to match the foreseen dimensions of the demonstration building: 10.2 m tall, 8.8 m wide, and 2.7 m deep. Two concrete slabs were installed at the first and second floor to perform all tests required for installing one CWM.

3.2. Installation of the CDPR

After the erection of the building, the DPAs, mobile platform, and control cabinet were brought to the building site. The top DPAs (2500 kg each) were installed on the building top floor by a mobile crane. The bottom DPAs (1100 kg each) were moved around using a forklift. Once the DPAs were installed, the necessary calibration was carried out.

Calibration of the drawing point positions was performed thanks to the integration of Total Station targets onto the swivel pulley assemblies. Each swivel pulley assembly featured four targets; their positions were used to build a local frame to reconstruct the current position of the associated drawing point. In order to calibrate the full system, apart from the A and B points, there were three Leica 360° targets [65] attached to the CDPR platform in order to track it on the move, three Leica 20 × 20 mm reflectors attached to the CDPR platform in order to calibrate the origin point of the MEE with respect to the CDPR platform frame, and at least three Leica 20 × 20 mm reflectors to triangulate the building from the Total Station. It was highly advisable to calibrate all the prism and reflectors at the same time to achieve best possible accuracy.

The calibration procedure was performed at the same time as the installation of the DPAs, with the drawing point positions being monitored continuously by a surveyor with a Total Station. The objective was to have the DPAs installed as close as possible to their theoretical positions: the distance to the theoretical positions was measured at maximum 19 mm.

After the installation of all the components of the CDPR, and before starting the final tests on the Acciona demonstration building, the measured positions of the targets and the corresponding A_i points (Fig. 24) were compared with the theoretical ones to verify that they were within the required tolerances. (See Fig. 25.)

3.3. Accuracy of the CDPR

Overall, the repeatability and accuracy of the CDPR platform were optimal in both demonstrations. The results of the first demonstration showed a better performance than expected in previous phases of the research project. The maximum position error of the CDPR was 22 mm and the maximum orientation error was approximately 0.8 degrees (see Table 3). Moreover, the preliminary results showed promising repeatability of the CDPR (with an accuracy of two to four mm, depending the location within the workspace and the wind load) while repeating the poses. Issues regarding looseness and stiffness of cable tension appeared in the corners of the workstations but did not undermine the stability of the platform.

3.4. Accuracy of the bracket installation

The deviations of the CDPR platform with respect to the desired position were planned to be adjusted by the MEE (see Fig. 26). On the first demonstration building, single brackets were installed according to planned locations. On the second demonstration building, a set of six brackets were placed during the tests according to a planned position. It was noted that the repeatability of the bracket placement only presented deviations of approximately 2 mm (see Fig. 26 where tests 1 to 5 are close to the planed location in blue dots), and thus, the capability of the system was guaranteed.

During the second demonstration, the calibration of the CDPR and the MEE platform was achieved with more precision. This permitted the installation of the brackets as in planned situations. The accuracy of the bracket placement was dependent on the calibration of the MEE with regard to the origin of the building and the CDPR platform. Moreover, the accuracy of the MEE depended on the accuracy of the Total Station.

It must be mentioned that the MEE did not present any relevant disturbances while it was stabilized by the grippers and that the robotic arm could perform its activities with the necessary firmness and without vibrations transferred from the CDPR. However, the robotic arm itself and the tools presented some level of vibrations while performing their work and in multiple drilling trials.

3.5. Accuracy of CWM installation

Some clarifications must be made to explain the results. The authors manually operated the CDPR for the placement of the CWM onto the brackets on the picking and placing. The authors had no previous experience of installing such CWM modules and this lack of experience likely affected the positioning accuracy. Moreover, the lower profile (close to points 13, 14 and 15 in Fig. 27) was fixed after the brackets were installed. Finally, the height of the CWM was adjusted manually once it was supported on the bracket. For these reasons, the final location of the CWM was more inaccurate than expected. Therefore, in the analysis of the results, it was necessary to adjust the planned point coordinates (see Table 4). Moreover, it was necessary to considered that during the measurements, the Total Station generated errors of up to 5 mm (this was accounted by measuring the same point several times by with the Total Station "stationed" on the same location).

The results in Table 4 reflect all the aforementioned issues. The deviations (*d*) are low especially in Points 1 to 12 but there are also significant errors in Points 13 to 15 (see also Fig. 27). In Table 4, $d\,z$ refers to deviations without considering errors on the z axis.

Considering that the major deviations were caused due to the aforementioned reasons, it can be stated that the overall accuracy of the systems was optimal, in general terms.

3.6. Time

With the tests carried out and the results achieved, the performance of the fully operational robotic system in real construction environments was foreseen (see attached Videos 1 to 4 and embedded videos in [36]). As in the following sections, the time consumption was monitored and analyzed. With the monitored tasks, the foreseen performance of the Hephaestus robot was deduced. The objective of such analysis was to compare it to the current manual methods for installing unitized curtain walls. It is important to differentiate the test realized in the context of the research project and the possible improved scenarios in the future. Construction sites differ from case to case and, therefore, the workspace of the CDPR needs to be adjusted to every case. Moreover, several workspaces are needed to cover the whole building. This point needs to be considered in the case of the implementation in real cases. First, the unitary time was measured. In Table 5, the time for installing the CDPR and the MEE is listed.

The whole bracket installation cycle was accomplished in 0.18 h (less than 11 min) and it is an operation that could be achieved by one operator (see Table 6). The question of using a robotic arm with so many changing tools is a topic that needs to be addressed in the future. The MEE could only host two brackets and its respective anchors. For this reason, the platform had to be fed with anchors every two operations, which added about one minute to the overall count.

Once all the brackets were installed, the CWMs needed to be placed in a magazine to facilitate the suction cups in the platform to reach them. This was an operation that required excessive logistic resources and operating time in demonstrations (see Table 7).

The future usability of the system will rely on the efficiency, productivity and suitability to the CWM installation process. Setting up the CDPR workspace is the most time-consuming activity among the different tasks. Therefore, it is necessary to maximize the use of the workspace. With the data gathered in Tables 5–7, the minimum size of workspace can be estimated to ensure competitiveness by using *Eq. (4)* (where *W* is the current installation time per m² with manual techniques, T_i is the installation time of the CDPR workspace, T_b is the installation time of the bracket, T_c is the installation time of the CWM, *f* is the number of floors, c_f is the number of CWM per floor and *A* is the area of each of the CWM).

$$W = \frac{T_i}{A \times f \times c_f} + \frac{T_b \times f\left(c_f + 1\right)}{A \times f \times c_f} + \frac{T_c \times f \times c_f}{A \times f \times c_f} \tag{4}$$

Where *W* is 0.48 h/m², and *A* is 4.8 m², and c_f is 20, *f* (number of floors) would be 4.8 (or a workspace of 96 m²). For instance, a facade of more than five floors and 20 CWM in each floor, the time spent by the CDPR and the MEE would be less than that with manual methods which is around 0.5 h/m² [66]. This data is significant for considering the integration of the CDPR in a construction site (see Fig. 28).

The trajectories and time to perform the different tasks to assemble the CWMs with the CDPR were compared with those done with current manual techniques and feasibility was analyzed [66].

4. Future needs and conclusions

The experiences and results carried out in real scenarios defined a path for future marketization of the Hephaestus robot. During the demonstrations, a few issues arose. In summary, these future needs for each sub-system shall be solved in the next research phases:

- **Sub-system 1:** Faster set up of the CDPR device is necessary. This is the main issue to solve before future marketization. As a first step for solving this main issue, a study was carried out to improve the logistics on the construction site (see Fig. 29)
- **Sub-system 2:** One of the issues regarding the bracket installation was the need to exchange several tools when the robotic arm was operating. Moreover, a more robust device for fixing the brackets needs to be achieved. In addition, the slab's non-planar situation was ignored. However, this is a topic that needs further consideration. Distance sensors would facilitate the recognition of the flatness of the slab.
- **Sub-system 3**: Recognition of the brackets before placing the CWM onto it. Moreover, a compliant connector that facilitates the placement of the connector will be necessary.

Apart from the points addressed in the conceptual framework's sub-systems, the Hephaestus robot was also used for dismantling CWMs (see attached Video 5) which opens the possibility for future uses as maintenance and repair of CWM facades.

However, there are still some points that need to be developed. In order to pursue future commercialization, market research was carried out which found a growing awareness from building owners and residents about comfort and health as well as political and economic drivers (e.g: nZEB and other EU directives, incentive schemes and favorable tax regimes, especially for green construction). Future marketability studies have also been carried out. In particular, based on a simplified cost-benefit analysis, Hu et al. concluded that the aforementioned CDPR for façade installation was theoretically worth investment in most EU countries as well as in the majority of G20 countries [66]. Technological innovations should complete these drivers, making investors, policy-makers and professionals (i.e. architects, designers as well as façade manufacturers) accelerate the adoption of construction robots.

In addition, technical standards contribute significantly and measurably to the economic growth and industrial output [67]. Back in the early 1990s, researchers already recognized the importance of standardization in construction robots [68]. However, standards specifically for construction robots have not been much developed due to various difficulties caused by the nature of construction sector. In order to further facilitate the commercialization of new device categories, standards can contribute in the following ways: 1) standardization of components and interfaces in order to allow for faster development and efficient supply chains ("interoperability"); 2) standardize the processes and infrastructures surrounding the new technology or product/service; and 3) ensure the quality and efficiency of the technology and/or its development processes in order to minimize the risks for the involved stakeholders. Therefore, the following roadmap in the follow-up project can be proposed to push forward the standardization of construction robots.

(1) An in-depth cross-disciplinary gap analysis needs to be conducted to understand the gaps in the existing standard landscape and a stakeholder network analysis needs to be conducted to identify the relevant stakeholders (Year 1);

(2) Establish a CEN workshop agreement (CWA) to determine the right strategy to develop the standards (Year 2);

(3) Initiate a technical committee at a standardization body to prioritize certain topics and arrange first working groups and standards projects within the TC (Year 3);

(4) Develop the standards and increase the number of working groups and standards within the technical committee (Year 4+).

Once the technical and normative gaps are resolved and a strong standardization process is achieved, similar systems such as the Hephaestus project could become part of the construction processes.

Declaration of Competing Interest

The authors declare that they have no known competing financial interests or personal relationships that could have appeared to influence the work reported in this paper.

Acknowledgements

Appendix A. Supplementary data

Supplementary data to this article can be found online at https://doi.org/10.1016/j.autcon.2022.104235.

References

[1] Beuth publishing DIN, EN 13830:2020–11, https://www.beuth.de/de/norm/din-en-13830/306849606, 2020.

[2] ISO, ISO 16283-3:2016, Acoustics — Field Measurement of Sound Insulation in Buildings and of Building Elements — Part 3: Façade Sound Insulation. https://www.iso.org/standard/59748.html, 2016 accessed March 30, 2021.

[3] ISO, ISO 717-1:2013, Acoustics — Rating of Sound Insulation in Buildings and of Building Elements — Part 1: Airborne Sound Insulation. https://www.iso.org/standard/51968.html, 2013 accessed March 29, 2021.

[4] ISO, ISO 10848-1:2017, Acoustics — Laboratory and Field Measurement of Flanking Transmission for Airborne, Impact and Building Service Equipment Sound between Adjoining Rooms — Part 1: Frame Document. https://www.iso.org/standard/67226.html, 2017 accessed March 29, 2021.

[5] T. Bock, K. Iturralde, Automated and robotic process lifecycle of prefabricated facades, in: Neue Entwicklungen Im Betonbau, Beuth Verlag GmbH, 2019, pp. 117–129. ISBN: 978–3–410-29067-4.

[6] H. Miyakawa, J. Ochiai, K. Oohata, T. Shiokawa, Application of automated building construction system for high-rise office building, in: M.-T. Wang (Ed.), Proceedings of the 17th IAARC/CIB/IEEE/IFAC/IFR International Symposium on Automation and Robotics in Construction, International Association for Automation and Robotics in Construction (IAARC), 2000, pp. 1–6, https://doi.org/10.22260/ISARC2000/0083.

[7] H. Miyakawa, J. Ochiai, K. Oohata, T. Shiokawa, Application of automated building construction system for high-rise office building, in: Proceedings of the International Symposium on Automation and Robotics in Construction, Taipei, 2000, ISBN 9789570266986, pp. 1–6, https://doi.org/10.22260/ISARC2000/0083.

[8] J. Maeda, Development and application of the SMART system, in: Automation and Robotics in Construction, 1994, pp. 457–464, https://doi.org/10.1016/B978-0-444-82044-0.50064-3.

[9] E. Gambao Galán, C. Balaguer, F. Gebhart, Robot assembly system for computer integrated construction, Autom. Constr. 9 (2000) 479–487, https://doi.org/10.1016/S0926-5805(00)00059-5.

[10] S. Lee, M. Gil, K. Lee, S. Lee, C. Han, Design of a ceiling glass installation robot, in: Proceedings of International Symposium on Automation and Robotics in Construction, 2007, pp. 247–252, https://doi.org/10.22260/isarc2007/0044.

[11] J. Činkelj, R. Kamnik, P. Čepon, M. Mihelj, M. Munih, Closed-loop control of hydraulic telescopic handler, Autom. Constr. 19 (7) (2010) 954–963, https://doi.org/10.1016/j.autcon.2010.07.012.

[12] C. Thompson, P.J. Campbell, Tendon Suspended Platform Robot, WO1995023053A1, https://patents.google.com/patent/WO1995023053A1, 1996.

[13] A. Pott, Cable-Driven Parallel Robots: Theory and Application, Springer, 2018, ISBN 978-3-319-76138-1, https://doi.org/10.1007/978-3-319-76138-1.

[14] C. Gosselin, Cable-driven parallel mechanisms: state of the art and perspectives, Mech. Eng. Rev. 1 (2014) 1–17, https://doi.org/10.1299/mer.2014dsm0004.

[15] T. Bruckmann, L. Mikelsons, T. Brandt, M. Hiller, D. Schramm, Wire robots part I: kinematics, analysis & design, in: J.-H. Ryu (Ed.), Parallel Manipulators, Intechopen, 2008, ISBN 978-3-902613-20-2, https://doi.org/10.5772/5365.

[16] J. Albus, R. Bostelman, N. Dagalakis, The NIST robocrane, J. Robot. Syst. 10 (1993) 709–724, https://doi.org/10.1002/rob.4620100509.

[17] R. Kurtz, V. Hayward, Dexterity measure for tendon actuated parallel mechanisms, in: International Conference on Advanced Robotics, 1991, ISBN 0-7803-0078-5, pp. 1141–1146, https://doi.org/10.1109/ICAR.1991.240402.

[18] M. Gouttefarde, J.-F. Collard, N. Riehl, C. Baradat, Geometry selection of a redundantly actuated cable-suspended parallel robot, IEEE Trans. Robot. 31 (2015) 501–510, https://doi.org/10.1109/TRO.2015.2400253.

[19] A. Pott, H. Mütherich, W. Kraus, V. Schmidt, P. Miermeister, A. Verl, in: T. Bruckmann, A. Pott (Eds.), IPAnema: a family of cable-driven parallel robots for industrial applications, cable-driven parallel robots, Springer, 2013, ISBN 978-3-642-31988-4, pp. 119–134, https://doi.org/10.1007/978-3-642-31988-4_8.

[20] L.L. Cone, Skycam-an aerial robotic camera system, Byte 10 (1985) 122–132. https://archive.org/details/byte-magazine-1985-10/page/n121/mode/2up.

[21] S.E. Landsberger, T.B. Sheridan, Parallel Link Manipulators. https://patents.google.com/patent/US4666362A/en, 1987.

[22] D. Culla, J. Gorrotxategi, M. Rodríguez, J.B. Izard, P.E. Hervé, J. Cañada, Full production plant automation in industry using cable robotics with high load capacities and position accuracy, in: Iberian Robotics Conference, Springer International Publishing, 2018, ISBN 978-3-319-70836-2, pp. 3–14, https://doi.org/10.1007/978-3-319-70836-2_1.

[23] PAR_systems, Tensile Truss. https://www.par.com/hazardous-environments/tensile-truss/, 2021 accessed September 21, 2021.

[24] T. Bruckmann, W. Lalo, C. Sturm, D. Schramm, M. Hiller, Design and realization of a high rack storage and retrieval machine based on wire robot technology, in: Proceedings of the International Symposium on Dynamic Problems of Mechanics, 2013, https://doi.org/10.1007/978-3-319-91217-2.

[25] Jaso Industrial Cranes, Cablebot. https://jasoindustrial.com/fr-fr/services/telechargements/cranebot-catalog.pdf, 2021 accessed September 21, 2021.

[26] J.-B. Izard, M. Gouttefarde, C. Baradat, D. Culla, D. Sallé, in: T. Bruckmann, A. Pott (Eds.), Integration of a parallel cable-driven robot on an existing building façade, cable-driven parallel robots, Springer, 2013, ISBN 978-3-642-31988-4, pp. 149–164, https://doi.org/10.1007/978-3-642-31988-4_10.

[27] A. Pott, C.A.V. Meyer, Large-scale assembly of solar power plants with parallel cable robots, in: International Symposium on Robotics and German Conference on Robotics, 2010, pp. 1–6. https://ieeexplore.ieee.org/document/5756909/metrics#metrics.

[28] P. Bosscher, R.L. Williams, L.S. Bryson, D. Castro-Lacouture, Cable-suspended robotic contour crafting system, Autom. Constr. 17 (2007) 45–55, https://doi.org/10.1016/j.autcon.2007.02.011.

[29] S. Schröder, Under constrained cable-driven parallel robot for vertical green maintenance, in: M. Gouttefarde, T. Bruckmann, A. Pott (Eds.), Proceedings of International Conference on Cable-Driven Parallel Robots, Springer, 2021, ISBN 978-3-030-75789-2, pp. 389–400, https://doi.org/10.1007/978-3-030-75789-2.

[30] I. Vukorep, Autonomous big-scale additive manufacturing using cable-driven robots, in: Proceedings of International Symposium on Automation and Robotics in Construction, 2017, pp. 254–259, https://doi.org/10.22260/ISARC2017/0034.

[31] T. Bruckmann, C. Reichert, M. Meik, P. Lemmen, A. Spengler, H. Mattern, M. König, Concept studies of automated construction using cable-driven parallel robots, in: Proceedings of the International Conference on Cable-Driven Parallel Robots, Springer International Publishing, 2018, ISBN 978-3-319-61431-1, pp. 364–375, https://doi.org/10.1007/978-3-319-61431-1_31.

[32] R. Boumann, P. Lemmen, R. Heidel, T. Bruckmann, Optimization of trajectories for cable robots on automated construction sites, in: Proceedings of the International Symposium on Automation and Robotics in Construction, 2020, pp. 465–472, https://doi.org/10.22260/ISARC2020/0065.

[33] J.-P. Merlet, A. Marionet, Family of Modular Wire-Driven Parallel Robots, Advances in Robot Kinematics: Motion in Man and Machine, Springer, Netherlands, 2010, ISBN 978-90-481-9262-5, pp. 53–61, https://doi.org/10.1007/978-90-481-9262-5_6.

[34] INRIA, Les larmes du prince : impression en 3D robotique art et vitrification. https://www.inria.fr/fr/les-larmes-du-prince-impression-en-3d-robotique-art-et-vitrification, 2021 accessed September 21, 2021.

[35] European Comission, Highly automatEd PHysical Achievements and PerformancES Using Cable roboTs Unique Systems. https://cordis.europa.eu/project/id/732513/de, 2017.

[36] Hephaestus_Consortium, Hephaestus - EU H2020 Project. https://www.hephaestus-project.eu/, 2017 accessed October 5, 2021.

[37] K. Iturralde, T. Linner, T. Bock, Development and preliminary evaluation of a concept for a modular end effector for automated/robotic facade panel installation in building renovation, in: Proceedings of the Onference on Advanced Building Skins, Bern, Switzerland, 2015 https://doi.org/https://abs.green/conference-proceedings.

[38] R.B. Marimont, A new method of checking the consistency of precedence matrices, J. Assoc. Comput. Mach. 6 (1959) 164–171, https://doi.org/10.1145/320964.320973.

[39] D.V. Steward, The design structure system: a method for managing the design of complex systems, IEEE Trans. Eng. Manag. (1981) 71–74, https://doi.org/10.1109/TEM.1981.6448589.

[40] N.P. Suh, Axiomatic Design: advances and applications, in: The Oxford Series on Advanced Manufacturing, 2001, ISBN 9780195134667.

[41] G. Altshuller, 40 Principles: TRIZ Keys to Innovation 1, Technical Innovation Center, Inc., 2002, ISBN 978-0964074033.

[42] G. Tennant, Six Sigma: SPC and TQM in Manufacturing and Services, Gower Publishing, Ltd., 2001, https://doi.org/10.4324/9781315243023. ISBN: 9781315243023.

[43] M. Taghavi, K. Iturralde, T. Bock, Cable-driven parallel robot for curtain wall modules automatic installation, in: Proceedings of the International Symposium on Automation and Robotics in Construction, 2018, pp. 396–403, https://doi.org/10.22260/ISARC2018/0056.

[44] H. Hussein, J. Cavalcanti-Santos, J.B. Izard, M. Gouttefarde, Smallest maximum cable tension determination for cable-driven parallel robots, IEEE Trans. Robot. 37 (2021) 1186–1205, https://doi.org/10.1109/TRO.2020.3043684.

[45] M. Gouttefarde, J. Collard, N. Riehl, C. Baradat, Simplified static analysis of large-dimension parallel cable-driven robots, in: IEEE International Conference on Robotics and Automation, 2012, pp. 2299–2305, https://doi.org/10.1109/ICRA.2012.6225159.

[46] Computers & Structures, I, SAP2000 CSI Analysis Reference Manual. https://www.csiamerica.com/products/sap2000, 2016 accessed October 5, 2021.

[47] Beuth Publishing DIN, EN 14492, Cranes - Power Driven Winches and Hoists - Part 2: Power Driven Hoists. https://www.beuth.de/de/norm/din-en-14492-2/297532061, 2019 accessed March 29, 2021.

[48] Beuth publishing DIN, EN 13001, Cranes - General Design - Part 1: General Principles and Requirements. https://www.beuth.de/en/standard/din-en-13001-1/232362571, 2015 accessed March 29, 2021.

[49] ISO, ISO 4301, Cranes — Classification — Part 1: General. https://www.iso.org/standard/63070.html, 2016 accessed March 29, 2021.

[50] ISO, ISO 16625, Cranes and Hoists — Selection of Wire Ropes, Drums and Sheaves. https://www.iso.org/standard/57301.html, 2013 accessed March 29, 2021.

[51] FEM, Technical Guidance. https://www.fem-eur.com/publications/technical-guidance/, 2021 accessed March 29, 2021.

[52] Beuth Publishing DIN, EN 12385, Steel Wire Ropes - Safety - Part 4: Stranded Ropes for General Lifting Applications. https://www.beuth.de/en/standard/din-en-12385-4/107301708, 2008 accessed March 29, 2021.

[53] Universal Robots, UR10. https://www.universal-robots.com/products/ur10-robot/, 2021 accessed September 30, 2021.

[54] G. El-Ghazaly, M. Gouttefarde, V. Creuze, F. Pierrot, Maximum wrench feasible payload in cable-driven parallel robots equipped with a serial robot, in: IEEE International Conference on Advanced Intelligent Mechatronics, 2016, pp. 1572–1578, https://doi.org/10.1109/AIM.2016.7576994.

[55] S. Garrido-Jurado, R. Muñoz-Salinas, F.J. Madrid-Cuevas, M.J. Marín-Jiménez, Automatic generation and detection of highly reliable fiducial markers under occlusion, Pattern Recogn. 47 (2014) 2280–2292, https://doi.org/10.1016/j.patcog.2014.01.005.

[56] M. Zavatta, Vision-Based Homing Procedure for an Overconstrained Cable-Driven Parallel Robot, University of Bologna, 2018. https://amslaurea.unibo.it/id/eprint/15298.

[57] M. Zavatta, M. Chianura, A. Pott, M. Carricato, A vision-based referencing procedure for cable-driven parallel manipulators, J. Mech. Robot. 12 (2020), https://doi.org/10.1115/1.4045745.

[58] Basler AG, Basler AG Homepage. https://www.baslerweb.com, 2021 accessed October 5, 2021.

[59] Nvidia, Harness AI at the Edge with the Jetson TX2 Developer Kit. https://developer.nvidia.com/embedded/jetson-tx2-developer-kit, 2021 accessed September 30, 2021.

[60] D. Illner, Daniel Illner's GitHub Page. https://github.com/frommwonderland/, 2021.

[61] Robot Operating System, Robot Operating System Homepage. https://www.ros.org/, 2021 accessed October 5, 2021.

[62] OpenCV, OpenCV Homepage. https://opencv.org/, 2021 accessed October 5, 2021.

[63] R. Hartley, A. Zisserman, Multiple View Geometry in Computer Vision, 2nd ed., Cambridge University Press, 2004 https://doi.org/10.1017/CBO9780511811685. ISBN: 9780511811685.

[64] Beckhoff, TwinCAT 3. https://www.beckhoff.com/en-en/products/automation/twincat/, 2021 accessed October 5, 2021.

[65] Leica Geosystems AG, Surveying Reflectors. https://leica-geosystems.com/, 2009 accessed October 5, 2021.

[66] R. Hu, K. Iturralde, T. Linner, C. Zhao, W. Pan, A. Pracucci, T. Bock, A Simple Framework for the Cost–Benefit Analysis of Single-Task Construction Robots Based on a Case Study of a Cable-Driven Facade Installation Robot, Buildings 11, 2021, pp. 1–8, https://doi.org/10.3390/buildings11010008.

[67] K. Blind, A. Jungmittag, A. Mangelsdorf, The Economic Benefits of Standardization. https://www.din.de/blob/89552/68849fab0eeeaafb56c5a3ffee9959c5/economic-benefits-of-standardization-en-data.pdf, 2011.

[68] J.-L. Salagnac, Construction robotics and standardization, in: T. Yoshino (Ed.), Proceedings of International Symposium on Automation and Robotics in Construction, International Association for Automation and Robotics in Construction (IAARC), 1992, pp. 161–164, https://doi.org/10.22260/ISARC1992/0022.